

## Transient Simulation of Ventilation Rate and Moisture load for Cold Attic Constructions - A CFD Analysis

*Master's Thesis in Applied Mechanics*

Ragnar Hellsvik

Department of Civil and Environmental Engineering  
CHALMERS UNIVERSITY OF TECHNOLOGY  
Gothenburg, Sweden 2015



REPORT NO. 2015:57

# Transient Simulation of Ventilation Rate and Moisture load for Cold Attic Constructions – A CFD Analysis

RAGNAR HELLSVIK

Department of Civil and Environmental Engineering  
CHALMERS UNIVERSITY OF TECHNOLOGY  
Gothenburg, Sweden 2015

Transient Simulation of Ventilation Rate and Moisture load for Cold Attic Constructions  
- A CFD Analysis  
RAGNAR HELLSVIK

©RAGNAR HELLSVIK, 2015.

Technical report no 2015:57  
Department of Civil and Environmental Engineering  
Chalmers University of Technology  
SE-412 96 Göteborg  
Sweden  
Telephone + 46 (0)31-772 1000

Cover:

Temperature contours for the attic model taken in a vertical plane parallel to the joists longitudinal direction in the middle of the attic.

This particular case was for four complete air displacements per hour and a temperature difference of  $\sim 25$  K.

Chalmers Reproservice  
Göteborg, Sweden 2015

Transient Simulation of Ventilation Rate and Moisture load for Cold Attic Constructions  
- A CFD Analysis  
RAGNAR HELLSVIK  
Department of Civil and Environmental Engineering  
Chalmers University of Technology

### **Abstract**

In this Master's thesis, numerical modeling of transient air, heat and mass transport is investigated in a principal cold attic construction through the use of the commercial CFD software ANSYS Fluent.

A numerical model that was developed and validated for steady state simulations in an earlier project is now being used for transient simulations over a total time of 24 hours to capture the daily variations in temperature and humidity levels.

The attic model contain wooden joists lying in a layer of insulation at the bottom of the attic, and a triangular shaped air cavity. Natural convection due to the temperature gradients between the hot floor and the cold roof along with forced convection driven by the ventilation system is investigated.

An hygrothermal analysis and numerical methods are applied to estimate the moisture load at the inner roof boundary for different ventilation rates.

The project has been performed as a collaboration between ÅF Industry AB and the Division of Building Technology at Chalmers University of Technology.

**Keywords:** Computational Fluid Dynamics, CFD, Building Physics, Heat transfer, Moisture Transport, Hygrothermal Analysis, Porous Media, Natural Convection, Forced Convection, Cold Attics

### **Sammanfattning**

I detta examensarbete har transient modellering av luft-, värme- och masstransport undersökts i en förenklad modell av en kallvindskonstruktion med hjälp av CFD-programvaran ANSYS Fluent.

En Numerisk modell som utvecklades och verifierades för fullt utvecklade strömningsförhållanden i ett tidigare projekt appliceras nu för transienta beräkningar över ett 24-timmarsintervall för att fånga dygnsvariationer i temperatur och luftfuktighet.

Modellen innehåller träbalkar som ligger längs golvet inuti ett isoleringslager, och en triangulärt formad luftspalt. Naturlig konvektion som uppstår p.g.a. temperaturgradienter mellan det varma golvet och det kalla taket tillsammans med påtvingad konvektion som drivs av ventilationssystemet inkluderas i modellen.

En hygrotermisk analys och numeriska metoder tillämpas för att estimera fuktbildning på undertaket för olika ventilationshastigheter.

Detta projekt har genomförts som ett samarbete mellan ÅF Industry AB och avdelningen för byggnadsteknologi på Chalmers tekniska högskola.

## Thesis Layout

This thesis work is based on the following research papers that have been submitted for publication in conferences and journals.

- *Transient Heat Transfer and Moisture Load in Cold Attic Constructions - A CFD Analysis*, V. Shankar, R. Hellsvik & C-E Hagentoft, submitted to the conference "6th International Conference on Energy Research and Development", March 14-16, 2016, State of Kuwait.
- *Transient Modeling of Heat Transfer and Evaporation in Cold Attics - A CFD Analysis*, V. Shankar, R. Hellsvik & C-E Hagentoft, submitted to the conference "IAQ 2016 Defining Indoor Air Quality: Policy, Standards and Best Practices", Sept. 12 – 14, 2016, Alexandria, VA.

## Acknowledgements

This Master's Thesis has been made in cooperation with the Department of Civil and Environmental Engineering at Chalmers University of Technology and ÅF Industry, Göteborg. I would like to show my gratitude to:

- My supervisor Vijay Shankar, Senior Consultant at ÅF Industry, who initiated the project and supported me through his guidance and assistance.
- ÅForsk, Ångpanneföreningens Forskningsstiftelse, for the scholarship that financed my visit to Atlanta and the 2015 ASHRAE Annual Conference.
- Carl-Eric Hagentoft and the Division of Building Technology at Chalmers University of Technology, for the opportunity to execute this project at Chalmers University of Technology.
- Paula Wahlgren, Senior Lecturer/Head of Division, Civil and Environmental Engineering, for her feedback and comments during the project.
- Tommie Månsson, PhD Student at the department of Civil and Environmental Engineering, for providing me with computational resources and valuable discussions.
- My family and friends who have supported me throughout my studies at Chalmers University of Technology.
- My opponent and friend Sathyavanan Chinnaswamy who, on short notice, read and analyzed my thesis report and provided me with professional feedback at the presentation seminar.

Ragnar Hellsvik, Göteborg 11/6/2015



## Abbreviations

<i>CFD</i>	Computational Fluid Dynamics
<i>DNS</i>	Direct Numerical Solution
<i>RANS</i>	Reynolds Averaged Navier-Stoke's
<i>EWFM</i>	Eulerian Wall Film Model
<i>VTT</i>	Valtion Teknillinen Tutkimuskeskus (State Technical Research Center)
<i>SIMPLE</i>	Semi-Implicit Method for Pressure-Linked Equations

## Nomenclature

$Re$	Reynolds number [-]
$Ra$	Rayleigh number [-]
$Ra_m$	Modified Rayleigh number [-]
$Nu$	Nusselt number [-]
$RH$	Relative Humidity [%]
$\rho$	Density [ $\text{kg}/\text{m}^3$ ]
$u_i$	Velocity [ $\text{m}/\text{s}$ ]
$p$	Pressure [ $\text{Pa}$ ]
$\tau_{ij}$	Viscous stress tensor [ $\text{kg}/(\text{m}\cdot\text{s}^2)$ ]
$g_i$	Gravitational acceleration [ $\text{m}/\text{s}^2$ ]
$U$	Internal energy [ $\text{m}^2/\text{s}^2$ ]
$c_p$	Specific heat [ $\text{J}/(\text{kg}\cdot\text{K})$ ]
$k_m$	Thermal conductivity [ $\text{W}/(\text{m}\cdot\text{K})$ ]
$T$	Temperature [ $\text{K}$ ]
$\mu$	Dynamic viscosity [ $\text{m}^2/\text{s}$ ]
$S_{ij}$	Strain-rate tensor [ $1/\text{s}$ ]
$\bar{u}$	Mean velocity [ $\text{m}/\text{s}$ ]
$L$	Characteristic length [ $\text{m}$ ]
$\nu$	Kinematic viscosity [ $\text{N}\cdot\text{s}/\text{m}^2$ ]
$\beta$	Coefficient of thermal expansion [ $1/\text{K}$ ]
$d_m$	Material thickness [ $\text{m}$ ]
$K$	Permeability [ $\text{m}^2$ ]
$q$	Heat flow rate per unit area [ $\text{J}/\text{m}^2$ ]
$v_s$	Humidity by volume at saturation [ $\text{g}_{h_2o}/\text{kg}_{air}$ ]

$v_e$	Humidity by volume of the ambient air [ $\text{g}_{h_2o}/\text{kg}_{air}$ ]
$v_i$	Humidity by volume in the living area [ $\text{g}_{h_2o}/\text{kg}_{air}$ ]
$v_a$	Humidity by volume in the attic space [ $\text{g}_{h_2o}/\text{kg}_{air}$ ]
$R_a$	Volume flow rate [ $\text{m}^3/\text{s}$ ]
$n$	Ventilation rate [1/h]
$T_{eq}$	Equivalent temperature [T]
$T_{amb}$	Ambient temperature [T]
$\psi_e, \psi_r$	Heat transfer coefficients [ $\text{W}/(\text{m}^2\text{K})$ ]
$\alpha_{sol}$	Absorptivity for solar radiation [-]
$I_{sol}$	Solar radiation energy [ $\text{W}/\text{m}^2$ ]
$M$	Density of moisture flow rate [ $\text{kg}/(\text{m}^2\text{s})$ ]
$r$	Latent heat of evaporation [J/kg]
$T^r$	Sky temperature [T]
$k$	Turbulent kinetic energy [ $\text{m}^2/\text{s}^2$ ]
$\varepsilon$	Turbulent dissipation rate [ $\text{m}^2/\text{s}^3$ ]
$\nu_T$	Turbulent viscosity [ $\text{m}^2/\text{s}$ ]
$u'$	Turbulent fluctuating velocity [m/s]
$Q$	Total heat flow rate [J]
$h$	Convective heat transfer coefficient [ $\text{W}/\text{K}\cdot\text{m}^2$ ]
$A$	Surface area [ $\text{m}^2$ ]
$\epsilon$	Emissivity [-]
$E$	Emissive power [ $\text{W}/\text{m}^2$ ]
$E_b$	Blackbody total emissive power [ $\text{W}/\text{m}^2$ ]
$\sigma$	Stefan-Boltzmann constant [ $\text{W}/(\text{m}^2\text{K}^4)$ ]
$\varphi$	Porosity [-]
$C_2$	Inertial resistance factor for porous zone [ $\text{m}^2/\text{kg}$ ]
$\alpha_k$	Volume fraction of phase $k$ [-]
$\dot{m}$	Mass flow rate [kg/s]
$H$	Water film thickness [m]
$\vec{V}$	Water film velocity [m/s]
$\dot{q}$	Source term due to droplet impingement to water film [ $\text{kg}/(\text{m}\cdot\text{s}^2)$ ]
$RH_{crit}$	Critical relative humidity [%]
$m$	Mold growth potential [-]
$G$	Incident radiation [ $\text{W}/\text{m}^2$ ]
$a$	Absorption coefficient [-]
$\sigma_s$	Scattering coefficient [-]
$C$	Linear-anisotropic phase function coefficient [-]

# Contents

<b>1</b>	<b>Introduction</b>	<b>1</b>
1.1	Previous Research . . . . .	2
1.2	Purpose . . . . .	3
1.3	Limitations . . . . .	4
<b>2</b>	<b>Theory</b>	<b>5</b>
2.1	Governing equations . . . . .	5
2.1.1	Continuity equation . . . . .	5
2.1.2	Momentum equation . . . . .	5
2.1.3	Energy equation . . . . .	5
2.2	Dimensionless numbers . . . . .	6
2.2.1	Reynolds number . . . . .	6
2.2.2	Modified Rayleigh number . . . . .	6
2.2.3	Nusselt number . . . . .	6
2.3	Relative Humidity . . . . .	6
2.4	Equivalent Roof temperature . . . . .	8
2.5	Turbulence modeling . . . . .	8
2.5.1	Standard $k$ - $\varepsilon$ model . . . . .	9
2.5.2	Realizable $k$ - $\varepsilon$ model . . . . .	9
2.6	The Boussinesq model . . . . .	10
2.7	Mechanisms of heat transfer . . . . .	10
2.7.1	Convection . . . . .	11
2.7.2	Conduction . . . . .	11
2.7.3	Radiation . . . . .	11
2.8	Modeling of fluid flow in porous media . . . . .	12
2.8.1	Porosity . . . . .	12
2.8.2	Darcy's law and Permeability . . . . .	12
2.8.3	Porous media in Fluent . . . . .	12
2.9	Moisture Transport . . . . .	12
2.9.1	Lagrangian Particle Tracking . . . . .	13
2.9.2	Eulerian-Eulerian Method . . . . .	13
2.9.3	The Eulerian Wall Film Model . . . . .	14
2.9.4	The VTT model for mold growth . . . . .	15
2.10	Radiative heat transfer in Fluent . . . . .	15
2.11	Boundary Conditions . . . . .	16
<b>3</b>	<b>Method</b>	<b>17</b>
3.1	Software . . . . .	17
3.2	Geometry . . . . .	17
3.3	Mesh . . . . .	19
3.3.1	Mesh Independence Study . . . . .	20
3.4	Fluent Settings . . . . .	23
3.4.1	Modeling the Insulation . . . . .	24
3.4.2	Boundary Conditions . . . . .	24
3.5	Running the Simulations . . . . .	26

<b>4 Results</b>	<b>28</b>
4.1 Paper 1 . . . . .	28
4.2 Paper 2 . . . . .	36
<b>5 Discussion and Conclusions</b>	<b>39</b>
5.1 Future Work . . . . .	40
<b>Appendices</b>	<b>43</b>
Paper 1: Transient Heat Transfer and Moisture Load in Cold Attic Constructions - A CFD Analysis	44
Paper 2: Transient Modeling of Heat Transfer and Evaporation in Cold Attics - A CFD Analysis	61

# 1 Introduction

Due to the increasing demands on energy efficient houses and the need for comfortable indoor climate conditions, buildings with cold attics are designed with, or retrofitted with thick insulation layers in the boundary between the living area and the cold attic space. Cold attics in highly insulated buildings, mainly in the southern and the west part of Sweden, often suffer from mold growth as a result of the micro climate and the present ventilation strategies of the air cavity. Moisture, heat and air transfer interact closely with each other and improving a building envelope's energy efficiency may lead to moisture-related problems [1].

Warm air of relatively high humidity levels might leak from the living areas through the insulation or through insufficiently sealed parts of the construction and water will then condensate at the cold surfaces as the air is cooled down. The ventilated outdoor air also contributes to the build up of moisture if the humidity of the outdoor air is high enough, and the micro climate in the attic is cold enough [2]. Mold related problems in cold attics and crawl spaces, such as rot and odors in indoor air, are directly related to high humidity levels and previous investigations have shown that the problems have been increasing in Sweden over the last decade. Cold attics and crawl spaces are pointed out to be the worst constructions in existing Swedish buildings with large existing and future mold problems [3].

Fluctuating levels of relative humidity due to annual and daily oscillations of the temperature within the attic makes it difficult to predict mold problems by field measurements. Short periods of high relative humidity does not cause risk for mold growth if the moisture of the structures are not increased for a longer time. E.g. Relative humidity of 95% for a couple of hours cause no harm if the continuous microclimate is below RH 75%, but relative humidity levels above 50% during winter conditions can cause condensation of moisture due to temperature fluctuations which drastically increases the risk of microbial growth [4].

Recent research have, on the other hand, shown that a greatly reduced or completely eliminated risk for mold growth can be achieved by installing a controlled mechanical ventilation system to the attic. [5] In such a solution an adaptive ventilation system is regulated with the in- and outdoor conditions as input, so that air is only let in if it has potential to enhance the indoor conditions (see Figure 1.1). In order to develop ventilation strategies for moisture safe attics, one must understand the different modes of heat transfer in building constructions. The transport of heat is generally divided into conductive, convective and radiative heat transfer which all play a role in the dynamics of the system. Convection is the transport of any media or property due to fluid motion, and can be divided into natural and forced convection. Natural convection is due to the fluid motion caused by density gradients, which in their turn are caused by the presence of temperature gradients. For forced convection the fluid motion is created by external forces from e.g. fans or pumps.

Convection is also the main source for transport of moisture which is a complex phenomenon to model in CFD (Computational Fluid Dynamics). Air and moisture might have to be treated as two separate phases in a multiphase formulation and there are many different ways to model multiphase flows depending on the characteristics of the flow. The objective of this thesis project is to find a suitable model for the moisture transport and investigate the physics of heat and mass transport in a typical cold attic construction by the use of transient CFD modeling. The results will then be used in a hygrothermal analysis in order to determine the risk of mold growth for different volume flow rates of air through the attic.

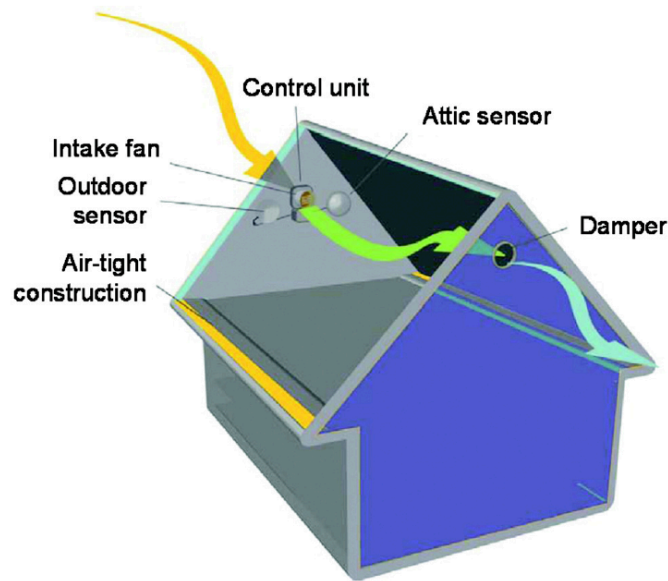


Figure 1.1: Cold attic with regulated ventilation. Picture taken from [5].

## 1.1 Previous Research

Field tests and extensive measurements of annual temperature and relative humidity levels were performed and compared with results from numerical models [5]. The risk for mold growth is estimated by determining a critical relative humidity level according to [6]. The field tests confirmed the simulation results, from which it has been shown that the risk for mold growth can be substantially reduced using adaptive ventilation systems.

The generation of turbulent plumes over heat sources in an indoor environment was numerically studied in [7] and the  $k$ - $\varepsilon$ -model was modified in two ways to correctly predict spreading rates of plumes in agreement with experiments. The standard production term due to buoyancy,  $G_B$ , was almost negligible because of the relatively small streamwise temperature gradients and was thus modified to include the temperature gradients in the lateral direction as well as the streamwise. Furthermore, the production term in the  $\varepsilon$ -equation was made more sensitive to irrotational strains in order to increase the lateral spreading rate of the plume.

The effect of natural convection on the thermal performance of porous insulation has been studied [8, 9] with the help of CFD. The combined effect of air movements inside the insulation and in the air cavity is studied and compared with experimental findings [8]. It is concluded that numerical methods for investigating the thermal properties of insulating medium with air cavity are of great practical interest, since the air movements in the air cavity considerably influences the thermal performance of the insulation [10].

A simplified model to evaluate the effects of air convection on the hygrothermal performance of buildings was developed in the study [11] on combined heat, air and moisture transport in building components. The model is validated by comparison with experimental data to evaluate the prediction of the thermal and moisture effects on air convection. The model treats air as an incompressible fluid but with varying

density which gives rise to buoyancy effects, and heat and moisture are transported by convection as well as diffusion. The experimental study to validate the model used a vertical cavity filled with expanded polyethylene sphere (EPS). It was concluded, by both numerical and measured data, that air convection increases the heat flow through the cavity as well as the dynamics of the moisture redistribution within the air cavity.

Different models for predicting moisture transport with wall condensation of water in convective flows has been investigated [12]. The possibilities of modeling condensation induced by a cold surface in flows of high velocities are investigated using the two commercial software ANSYS Fluent and ANSYS CFX. Stability of the simulations showed to be greatly affected by the material properties for water vapor, and real gas properties to define the water vapor material properties showed to be important to avoid unphysical results. The available condensation models as well as Euler-Euler multiphase models are presented and evaluated for the two solvers. The condensation model in ANSYS CFX is pointed out to be the appropriate choice when it comes to validity and complexity and for ANSYS Fluent it is recommended to use the Eulerian-Eulerian multiphase model with condensation and the Eulerian wall film model enabled.

In a previous thesis project [13] in 2014, the influence of natural and forced convection in a cold attic space with an underlying layer of insulation material was investigated for steady state simulations of single phase flow in ANSYS Fluent. Three different ventilation rates, in terms of complete air displacements per hour, and different temperatures at the roof boundary were investigated. The relation between the Nusselt number and the modified Rayleigh number (See Section 2) were plotted and compared with results from an experimental study performed by Mihail Serkitjis [17].

The insulation region is defined as a porous zone which means that an additional momentum equation is added to the flow equations within the insulation. Investigations proposed for future work in [13] are summarized below:

- Investigation of moisture transport
- Inclusion of multiphase modeling
- Treatment of radiation in the insulation

## 1.2 Purpose

The previous research [14] in 2014 was performed using a 3D model of a square box with an air cavity and an underlying insulation layer to validate CFD results of convective heat transfer with and without radiation by comparison with earlier experimental results from the PhD thesis by Mihail Serkitjis [17].

The main purpose of this thesis project is to include moisture transport for transient simulations with the CFD model developed in [14] and the same attic model that was used during the previous thesis [13, 15, 16]. The model has already been validated by comparison with experimental results and is therefore being used in this project as well. This means that a suitable model for moisture transport available in ANSYS Fluent will be chosen and investigated.

The first objective of the project will be to modify and improve the model that was used in [13, 15, 16]. The geometry of the wind deflectors will be modified since the ventilated airflow in the previous model tended to attach to the inner roof. Also, the inlet-outlet-configuration will be changed, which means that the top of the roof will be sealed and that one of the previous inlets will be changed to outlet. Finally, different numerical schemes and under relaxation factors in fluent will be used in order to achieve better convergence since the previous simulations gave rather high continuity residuals (order of  $10^{-1}$ ).

ANSYS Fluent is a well known and robust commercial CFD software with many different applications but it is not widely used in building physics. It is of interest to investigate how the code performs for low velocity flows with natural and forced convection.

This thesis project is divided into two studies. In the first study, mathematical models derived from extensive experiments will be used to estimate the risk for mold growth. In the second study a numerical condensation model in Fluent is used to investigate condensation and evaporation at the inner roof boundary of the attic. The overall results are summarized in Section 4 and more detailed results are found in two articles attached in the appendices of this report.

### **1.3 Limitations**

Since this project is a master's thesis performed by one student with approximately seventeen weeks assigned, time is the main limitation of the project. For this reason, the objective of the thesis is to investigate the performance of the available options for modeling of moisture transport in ANSYS Fluent rather than optimizing the hygrothermal performance of the attic design. Moisture transport combined with condensation is a complex phenomena and the main objective is to enhance the knowledge of the available modeling tools and to explore the impact of local climatic conditions.

Furthermore, The available academic license available at Chalmers restricts the number of computational cells to 512000 which limits the accuracy of the simulations.

## 2 Theory

This chapter includes the governing equations of the finite volume method, turbulence and multiphase modeling, dimensionless numbers, and the implementation of the equations in ANSYS Fluent.

### 2.1 Governing equations

The statement of the conservation laws of physics in fluid flow is represented by the governing equations. These laws states that the mass of a fluid is conserved, That the rate of change of momentum equals the sum of forces acting on a fluid element, and that the rate of change of energy is equal to the sum of the rate of work done on a fluid element and the rate of heat addition.

When the continuum assumption is applied, the fluid is treated as a continuous medium which means that molecular motions and interactions are neglected. Instead, the flow field is described in terms of macroscopic properties, e.g. temperature, density, pressure and velocity, and their time and space derivatives [19].

#### 2.1.1 Continuity equation

The conservation of mass is described by the three dimensional continuity equation for a compressible fluid:

$$\frac{\partial \rho}{\partial t} + \frac{\partial \rho u_i}{\partial x_i} = 0 \quad (2.1)$$

where the first term on the left hand side is the rate of change of density with time. The second term describes the net mass flow of the element across its boundaries. [20]

#### 2.1.2 Momentum equation

According to Newton's second law the rate of change of momentum of any particle is equal to the sum of forces acting on it. This is described by the Momentum equation which is also known as the Navier Stoke's equations. [20]

$$\frac{\partial u_i}{\partial t} + u_j \frac{\partial u_i}{\partial x_j} = -\frac{1}{\rho} \frac{\partial p}{\partial x_i} + \frac{1}{\rho} \frac{\partial \tau_{ji}}{\partial x_j} + g_i \quad (2.2)$$

#### 2.1.3 Energy equation

The transport equation for internal energy  $U$  in an incompressible fluid with constant  $c_p$  reads: [21]

$$\rho \frac{dU}{dt} = -p \frac{\partial u_i}{\partial x_i} + \Phi + \frac{\partial}{\partial x_i} \left( k_m \frac{\partial T}{\partial x_i} \right) \quad (2.3)$$

where

$$\Phi = 2\mu S_{ij}S_{ij} - \frac{2}{3}\mu S_{ii}S_{kk} \quad (2.4)$$

and  $S_{ij}$  is the strain-rate tensor defined as:

$$S_{ij} = \frac{1}{2} \left( \frac{\partial u_i}{\partial x_j} + \frac{\partial u_j}{\partial x_i} \right) \quad (2.5)$$

## 2.2 Dimensionless numbers

In this section the relevant dimensionless numbers are presented.

### 2.2.1 Reynolds number

The Reynolds number is the ratio of inertia forces and the viscous forces acting in a fluid:

$$Re = \frac{\bar{u}L}{\nu} = \frac{\rho\bar{u}L}{\mu} \quad (2.6)$$

where  $\nu$  is the kinematic viscosity and  $\mu$  is the dynamic viscosity of the fluid.  $\bar{u}$  and  $L$  are the mean flow velocity and some characteristic length of the flow geometry respectively. When the inertia forces are high in comparison to the viscous forces the flow is likely to be turbulent, and a large Reynolds number is therefore an indication of turbulence being present, and the opposite characterizes laminar flow. The critical Reynolds numbers which represent the transition from laminar to turbulent flow differ depending on the geometry and the properties of the fluid [22].

### 2.2.2 Modified Rayleigh number

The Rayleigh number,  $Ra$ , is a dimensionless number associated with buoyancy driven flows. When the Rayleigh number is below some critical value specific for the fluid, the heat transfer process is primarily conductive. When the Rayleigh number exceeds that critical value there is an onset of convective heat transfer. For porous media, such as insulation materials in attics, the *Modified Rayleigh number*,  $Ra_m$ , is often used to describe convection. The modified Rayleigh number can be regarded as a measure of the driving forces for convection.

$$Ra_m = \frac{\rho c_p g \beta d_m K \Delta T}{\nu k_m} \quad (2.7)$$

Where  $K$  and  $k_m$  are the air permeability and thermal conductivity respectively, of the porous material.  $\beta$ ,  $\nu$ ,  $\rho$  and  $c_p$  are the heat expansion coefficient, the kinematic viscosity, the density and the specific heat capacity, respectively, of the fluid.  $d_m$  is the thickness of the insulation and  $\Delta T$  is the temperature difference across it. [23]

### 2.2.3 Nusselt number

The Nusselt number is used to determine whether convection takes place in the heat transfer process. It is the ratio between the total heat flux (conduction and convection) and the conductive heat flux. The critical Nusselt number is 1 which represents the onset of convection. A large Nusselt number indicates that convection is the dominant heat transfer process. [23]

$$Nu = \frac{q_{conduction} + q_{convection}}{q_{conduction}} \quad (2.8)$$

## 2.3 Relative Humidity

The moisture content in air,  $v$ , is the mass of water per unit volume of air. The humidity by volume at saturation,  $v_s$  is a function of the local temperature and can be described with the equation below:

$$v_s = \frac{a \cdot \left(b + \frac{T}{100}\right)^c}{461.4 \cdot (T + 273.15)} \quad (2.9)$$

where  $a$ ,  $b$  and  $c$  are constants that take different values within different temperature intervals [26]. The values of the temperature are given in degrees Celsius. When  $v$  and  $v_s$  are known the relative humidity is calculated as

$$RH = \frac{v}{v_s} \quad (2.10)$$

For a cold attic application there are two main sources that contribute to the moisture content in the air within the attic space:

- The humidity by volume of the ventilated outdoor air,  $v_e$
- and the humidity by volume of leakage of the indoor air,  $v_i$

$$v_i = v_e + \Delta v \quad (2.11)$$

where  $\Delta v$  is the difference in water content between the outdoor and indoor air. The total water content in the attic air space,  $v_a$ , is then calculated as

$$v_a = v_e + \Delta v \frac{R_{a,i}}{R_{a,e} + R_{a,i}} \quad (2.12)$$

where  $R_{a,e}$  is the volume flow rate of outdoor air through ventilation, and  $R_{a,i}$  is the volume flow rate of indoor air through leakage.  $R_{a,i}$  is in this study approximated to be 10% of the ventilation rate of air in the living area which, in turn is approximated to be 0.5 complete air displacements per hour.  $\Delta v$  is usually in the range of 2-4 g/m<sup>3</sup> for residential houses [26] (3 g/m<sup>3</sup> was used in this study). The increase in the humidity level due to contributions from the living area for different ventilation rates is given in Table 2.1.

**Table 2.1:** Additional moisture for different ventilation rates

Ventilation rate, $n$	$v_a - v_e$
2	0.3107 g <sub>h<sub>2</sub>O</sub> /kg <sub>air</sub>
4	0.1638 g <sub>h<sub>2</sub>O</sub> /kg <sub>air</sub>
8	0.0842 g <sub>h<sub>2</sub>O</sub> /kg <sub>air</sub>

The final relative humidity in the attic is then given as:

$$RH = \frac{v_a}{v_s} \quad (2.13)$$

The measured levels of humidity by volume are shown in Figure 2.1. Since this sample of measured data is not cyclic over the 24-hour interval it cannot be considered to represent the normal levels for this time of the year. It was therefore chosen to also do the hygrothermal analysis with the average humidity level of April as input in order to get results that can represent the general climatic conditions of the month.

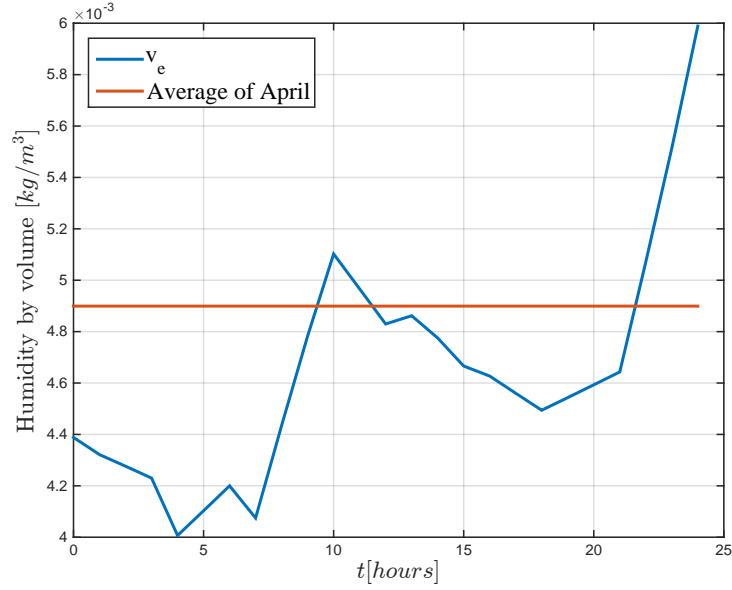


**Figure 2.1:** The humidity level,  $v_e$ , for the chosen day versus time plotted along with the average humidity level for April

## 2.4 Equivalent Roof temperature

In order to set reasonable boundary conditions for the CFD-model the effects of convection, long wave radiation, solar radiation and transfer of condensation/evaporation heat has to be included when defining the Dirichlet boundary condition for the external roof boundary. Otherwise the roof will have the same temperature as the ventilated air which is not the case in most situations. During a night with clear sky the roof has a heat exchange with the sky which has a lower temperature than the ambient air. Through long wave radiation the roof temperature can go below the limit where water starts to condense at the surface. During a day with clear sky the opposite effect is present due to solar radiation. [26] These effects are necessary to include in the CFD-model and the equivalent temperature,  $T_{eq}$ , can be calculated as:

$$T_{eq} = T_{amb} + \frac{1}{\psi_e} (I_{sol} \cdot \alpha_{sol} + M \cdot r + (T^r - T_{amb}) \cdot \psi_r) \quad (2.14)$$

where  $T_{amb}$  and  $T^r$  are the ambient air temperature and the sky temperature respectively.  $\alpha_{sol}$  is the absorptivity for solar radiation and  $\psi_r$  is the heat transfer coefficient for long wave radiation.  $\psi_e$  is an effective heat transfer coefficient, which is the sum of the convective,  $\psi_c$ , and the radiative one.  $M \cdot r$  is the transfer of latent heat, where  $M$  is the density of the moisture flow rate and  $r$  is the latent heat of evaporation.

## 2.5 Turbulence modeling

Solving the Navier-Stoke's equations without time or spatial averaging results in a complete flow field containing information at all scales. This is called DNS (Direct Numerical solution), which is very rare since the mesh has to be fine enough to capture the smallest scales of the flow field and this makes the calculations extremely computationally expensive. To afford simulations of larger domains, some of the

unknown turbulent properties of the flow are instead modeled, which results in a calculated flow field with less information. There is always a trade of between computational resources and level of information and in most cases it is accepted to get less information in order to simulate larger geometries. The sharp gradients prevailing at wall boundaries require a very high grid resolution to be resolved. It is therefore convenient to assume that the nature of the flow near the walls behave as in a fully developed turbulent boundary layer. The grid resolution can then be rougher by employing wall functions with prescribed boundary conditions. Several different turbulence models exist and in this thesis project, the Realizable  $k$ - $\varepsilon$  model has been used. [20, 21]

### 2.5.1 Standard $k$ - $\varepsilon$ model

The standard  $k$ - $\varepsilon$  model is a two-equation model where the transport equations for turbulent kinetic energy,  $k$ , and the dissipation rate,  $\varepsilon$ , are solved. It is based on the Reynolds averaged Navier-Stoke's equations (RANS). This model is popular because it provides acceptable accuracy for a wide range of CFD-applications at a low computational cost. [20, 21]

The transport equations of turbulent kinetic energy in the standard  $k$ - $\varepsilon$  model reads:

$$\frac{\partial k}{\partial t} + \langle u_j \rangle \frac{\partial k}{\partial x_j} = \nu_T \left[ \left( \frac{\partial \langle u_i \rangle}{\partial x_j} + \frac{\partial \langle u_j \rangle}{\partial x_i} \right) \frac{\partial \langle u_i \rangle}{\partial x_j} \right] - \varepsilon + \frac{\partial}{\partial x_j} \left[ \left( \nu + \frac{\nu_T}{\sigma_k} \right) \frac{\partial k}{\partial x_j} \right] \quad (2.15)$$

and the transport equation for the dissipation reads:

$$\frac{\partial \varepsilon}{\partial t} + \langle u_j \rangle \frac{\partial \varepsilon}{\partial x_j} = C_{\varepsilon 1} \nu_T \frac{\varepsilon}{k} \left[ \left( \frac{\partial \langle u_i \rangle}{\partial x_j} + \frac{\partial \langle u_j \rangle}{\partial x_i} \right) \frac{\partial \langle u_i \rangle}{\partial x_j} \right] - C_{\varepsilon 2} \frac{\varepsilon^2}{k} + \frac{\partial}{\partial x_j} \left[ \left( \nu + \frac{\nu_T}{\sigma_\varepsilon} \right) \frac{\partial \varepsilon}{\partial x_j} \right] \quad (2.16)$$

Where  $\nu_T$  is the turbulent viscosity:

$$\nu_T = C_\mu \frac{k^2}{\varepsilon} \quad (2.17)$$

The model contains several closure coefficients which are given in table 2.2 [20]. The standard  $k$ - $\varepsilon$

**Table 2.2:** Constant coefficients of the standard  $k$ - $\varepsilon$  model

Constant	Value
$C_\mu$	0.09
$C_{\varepsilon 1}$	1.44
$C_{\varepsilon 2}$	1.92
$\sigma_k$	1.00
$\sigma_\varepsilon$	1.30

model is the most widely used two-equation model due to its robustness and overall functionality. It is, however, not always giving good accuracy. The standard model was derived and tuned for high Reynolds number flows in which the turbulence is nearly isotropic. The constants in the model are set to give a good compromise for a wide range of different flow situations and the accuracy of the model can therefore be improved by adapting the coefficients to specific experiments. [20]

### 2.5.2 Realizable $k$ - $\varepsilon$ model

The realizable  $k$ - $\varepsilon$  model is a modified version of the standard  $k$ - $\varepsilon$  model where the  $k$  equation has been corrected. In the standard model the normal stresses can become negative for flows with large mean

strain rates. This is done by using a realizability constraint on the predicted stress tensor. The normal components of the Reynolds stress tensor, which by definition must be larger than zero, are modeled as:

$$\langle u'_i u'_i \rangle = \sum_i \langle u'^2_i \rangle = \frac{2}{3}k - 2\nu_T \frac{\partial \langle u_i \rangle}{\partial x_j} = \frac{2}{3}k - 2C_\mu \frac{k^2}{\varepsilon} \frac{\partial \langle u_i \rangle}{\partial x_j} \quad (2.18)$$

If the negative term including  $C_\mu$  becomes large enough the normal stress will turn negative. In the Realizable  $k$ - $\varepsilon$  model the  $C_\mu$ -coefficient is taken as a function of the local state of the flow to make sure that the normal stress stays positive.

The realizable model also contains a modification of the  $\varepsilon$ -equation where a production term for turbulent energy dissipation is included. Previous research shows that the realizable model performs better than the standard one in complex flows, such as boundary layer flows, separated flows and rotating shear flows [20]. The transport equations in the realizable  $k$ - $\varepsilon$  model are, except for the modifications described above, the same as for the standard model.

## 2.6 The Boussinesq model

For buoyancy driven flows the density variations due to temperature gradients give rise to fluid motions. An intuitive way to solve buoyancy driven flows would be to set the fluid density as a function of its temperature, but it is possible to get faster convergence by modeling the buoyancy effects using the Boussinesq model. This model uses a constant value of the density in all solved equations except for the buoyancy term in the momentum equation: [24].

$$(\rho - \rho_0) \approx -\rho_0 \beta (T - T_0) \quad (2.19)$$

Here,  $\rho_0$  is the constant density of the fluid,  $T_0$  is the operating temperature and  $\beta$  is the coefficient of thermal expansion. This relation is obtained from the Boussinesq approximation:

$$\rho = \rho_0 (1 - \beta \Delta T) \quad (2.20)$$

The Boussinesq model is a good approximation when the temperature differences in the domain are small  $\beta(T - T_0) \ll 1$ . [24]

## 2.7 Mechanisms of heat transfer

There are three different heat transfer modes:

- Convection
- Conduction
- Radiation

The driving force for all of these mechanisms is a difference in temperature, and when a temperature gradient is present heat will spontaneously be transferred from the warmer region to the colder [22]. Only if work is done on a system will it be possible for heat to flow from a cold region to a warm one (*Second law of thermodynamics*).

### 2.7.1 Convection

Convection is the transport of thermal energy, stored in particles or molecules within a fluid, caused by the fluid motion. Newton's law of cooling describes the convective heat transfer from a solid surface to its surroundings:

$$\frac{d}{dt}(Q_{convection}) = hA(T_s - T_\infty) \quad (2.21)$$

where  $h$  is the convective heat transfer coefficient, which in equation 2.21 is assumed to be independent of the temperature difference between the surface and its surroundings.  $A$ , [ $m^2$ ], is the surface area of the solid boundary,  $T_s$ , [ $K$ ], is the surface temperature and  $T_\infty$  is the temperature of the surrounding fluid far from the solid surface.

Convection itself can be divided into forced and natural convection, where forced convection is when the motion of the fluid is driven by external forces form e.g. fans or pumps. In natural convection the fluid motion is driven by temperature differences in the domain, giving rise to density gradients. [22]

### 2.7.2 Conduction

Conductive heat transfer is the dispersion of heat in a matter of any form due to interaction of particles. In solid materials the conductive heat transfer is caused by the spreading of molecule vibrations and by the transportation of free electrons within the material. In fluids and gases, it is driven by collisions and diffusion of molecules. Fourier's law [22], in its one dimensional form describes steady heat transfer in one direction:

$$q_{conduction} = -k_m \frac{dT}{dx} \quad (2.22)$$

which is used for simple applications. Here,  $q_{conduction}$  is the heat transfer rate per square meter.  $k_m$  is the thermal conductivity of the of the material. [22]

### 2.7.3 Radiation

The third mode of heat transfer, Radiation, is the process where electromagnetic waves are emitted by matter from one surface to another. Radiative heat transfer does not require any medium between the surfaces, as for convection and conduction. It does, however, require surfaces that can exchange radiative heat. All surfaces at a temperature above absolute zero emit thermal radiation. Two relevant parameters for radiative heat transfer are the *Stefan-Boltzmann* constant and the *emissivity* of a material. The emissivity is defined as the ratio between the real emissive power,  $E$ , of a material and the blackbody total emissive power,  $E_b$ . [26]

$$\epsilon = \frac{E(T)}{E_b(T)} \quad (2.23)$$

The blackbody total emissive power is defined as

$$E_b = \sigma T^4 \quad (2.24)$$

where  $\sigma$  is the Stefan-Boltzmann constant.

$$\sigma = 5.67 \cdot 10^{-8} \text{ W/m}^2 \text{K}^4 \quad (2.25)$$

The net radiative heat transfer from a surface to its surroundings is calculated as

$$\frac{d}{dt}(Q_{radiation}) = \epsilon \sigma A(T_s^4 - T_{sur}^4) \quad (2.26)$$

where  $A$  is the surface area of the body.  $T_s$  and  $T_{sur}$  are the absolute temperatures of the body and the surrounding surface respectively. [22]

## 2.8 Modeling of fluid flow in porous media

This section describes the relevant concepts and equations for fluid flow through porous media

### 2.8.1 Porosity

The porosity,  $\varphi$ , of a material is defined as the fraction of the total volume that is occupied by voids (air). The fraction of the volume which is occupied by solid material is thus  $1 - \varphi$ . By defining it this way it is assumed that the whole void space is connected. [27]

### 2.8.2 Darcy's law and Permeability

Darcy's law describes the permeability of a material with unidirectional flow:

$$\nabla p = -\frac{\mu}{K}u_i \quad (2.27)$$

where  $\mu$  is the dynamic viscosity,  $K$  is the permeability,  $\nabla p$  is the pressure gradient and  $u_i$  is the seepage velocity. For a one dimensional steady case:

$$u = -\frac{K}{\mu} \frac{dp}{dx} \quad (2.28)$$

The permeability is a measure of the fluid's ability to penetrate the porous medium, and a low value of the permeability indicates a large flow resistance. The value of the permeability is geometry-dependent. [23, 27]

### 2.8.3 Porous media in Fluent

In Ansys Fluent the properties of the porous media are modeled by the implementation of an extra source term in the momentum equations. The part of the domain that is filled by insulation material is defined as a so called porous zone in which these modifications are implemented. The additional source term reads:

$$S_i = \left( \frac{\mu}{K}u_i + C_2 \frac{1}{2} \rho |u| u_i \right) \quad (2.29)$$

where the first term on the right hand side represents the viscous losses according to Darcy's law, and the second one represents the inertial losses.  $C_2$  is the inertial resistance factor, which for laminar flow can be assumed to be zero since the viscous forces are dominant in such cases. [24]

## 2.9 Moisture Transport

In this section, different approaches for treating multiphase flows are presented. Mixtures of different phases (gas/liquid/solid/) as well as mixtures of immiscible fluids are classified as multiphase flows and great importance lies in determining a suitable model for the present case, since the mesh density and time step size are chosen differently between the models. Generally, multiphase flows can be divided into flows where the phases are separated and flows where they are dispersed.

### 2.9.1 Lagrangian Particle Tracking

The Lagrangian particle tracking method, or the Eulerian-Lagrangian method, is used for dispersed flows where the dispersed phase is treated as particles surrounded by a continuous fluid phase. The flow in the continuous phase is solved with the traditional governing equations and the discrete particles are tracked by determining the forces, and applying Newton's second law on each particle:

$$m_p \frac{du_{i,p}}{dt} = F_{i,Drag} + F_{i,Lift} + F_{i,Press} + F_{i,Virt} + F_{i,History} + F_{i,Buoy} + F_{i,Therm} + F_{i,Turb} + F_{i,Brown} \quad (2.30)$$

- $F_{i,Drag}$  is the drag force determined from the relative velocity between the particle and its environment.
- $F_{i,Lift}$  is the force parallel to the gravitation as a result of a velocity gradient in its direction.
- $F_{i,Press}$  is the pressure and shear force acting on the particle's surface
- $F_{i,Virt}$  is the Virtual mass (or Apparent mass) force which is the force acting on the particle as a result of relative accelerations between the particle and the continuous phase. It can be regarded as the additional mass that the particle appears to have as its velocity and/or the surrounding fluid's velocity is changed.
- $F_{i,History}$  describes the viscous effects of acceleration of the relative velocities due to development of the boundary layer.
- $F_{i,Buoy}$  is the buoyant force acting on the particle due to the difference in density between the dispersed and continuous phase.
- $F_{i,Therm}$  is the thermophoretic force which is generated by temperature gradients in the continuous phase.
- $F_{i,Turb}$  is the force due to turbulence in the continuous phase modeled by addition of random velocity fluctuations to the mean velocity.
- $F_{i,Brown}$  is the Brownian force which describes the effect of random molecular collisions.

In Lagrangian Particle Tracking models the phases can exchange heat, mass and momentum. These models are recommended for flows with low volume fraction of the dispersed phase. A necessary requirement for the model to work properly is that the particles has to be much smaller than the elements of the mesh. Different levels of coupling between the phases are implemented as source terms depending on the flow situation. [18, 20, 29]

### 2.9.2 Eulerian-Eulerian Method

The Eulerian-Eulerian method treats all phases as continuous phases that interact by the exchange of heat, mass and momentum. It is therefore often referred to as a two-fluid model. This framework is used to model both stratified and dispersed flows and is less computational intensive than Eulerian-Lagrangian models due to a greater level of averaging. This of course results in solutions containing less information. It is derived by volume or ensemble averaging and one important quantity that arises from the averaging is the volume fraction  $\alpha_k$ . The equations for the two-fluid models for each phase read:

$$\sum_k \alpha_k = 1 \quad (2.31)$$

$$\frac{\partial \alpha_k \rho_k}{\partial t} + \frac{\partial \alpha_k \rho_k u_{i,k}}{\partial x_i} = - \sum_{l=1}^I (\dot{m}_{kl} - \dot{m}_{lk}) \quad (2.32)$$

$$\frac{\partial \alpha_k \rho_k u_{i,k}}{\partial t} + \frac{\partial \alpha_k \rho_k u_{i,k} u_{j,k}}{\partial x_j} = -\alpha_k \frac{\partial p}{\partial x_i} + \frac{\partial \alpha_k \tau_{ij,k}}{\partial x_k} + \alpha_k \rho_k g_i + F_{i,k} \quad (2.33)$$

where  $k$  represents each phase and  $I$  in the continuity equations represents the number of present phases.  $\dot{m}_{lk}$  is the mass transport from phase  $l$  to phase  $k$ , and  $F_k$  in the momentum equations is the interaction force with other phases. [20]

### 2.9.3 The Eulerian Wall Film Model

The Eulerian Wall Film model (EWFm) is a model which is used to estimate the creation and flow of liquid films that build up on wall surfaces. A liquid film is formed as fluid droplets impinge the solid surface and the outcome of the impingement is different depending on the energy of the incoming droplet. This model is to be used when the thickness of the film is small compared to the radius of the surface curvature, and when the film is thin enough so that the flow within the film can be assumed to be parallel to the surface.

The fundamental picture of a film model consists of a two dimensional liquid film and the foundation of the EWFm formed by the governing equations for conservation of mass and momentum. For a two dimensional Wall Film in a three dimensional domain the conservation of mass reads:

$$\frac{\partial H}{\partial t} + \nabla_s \cdot [H \vec{V}_l] = \frac{\dot{m}_s}{\rho_l} \quad (2.34)$$

where  $H$  is the height of the film,  $\nabla_s$  is the surface gradient operator,  $\vec{V}_l$  is the mean film velocity,  $\rho_l$  is the density of the liquid and  $\dot{m}_s$  is the mass source per unit wall area due to incoming droplets, film separation, film stripping and phase change.

The conservation of film momentum reads:

$$\frac{\partial H \vec{V}_l}{\partial t} + \nabla_s \cdot (H \vec{V}_l \vec{V}_l) = -\frac{H \nabla_s p_L}{\rho_l} + (\vec{g} \cdot \vec{\tau}) H + \frac{3}{2\rho_l} \vec{\tau}_{fs} - \frac{3\nu_l}{H} \vec{V}_l + \frac{\dot{q}}{\rho_l} \quad (2.35)$$

where

$$p_L = p_{gas} + p_h + p_\sigma = p_{gas} + (-\rho H (\vec{n} \cdot \vec{g})) + (-\sigma \nabla_s \cdot (\nabla_s H)) \quad (2.36)$$

The terms on the left hand side in equation 2.35 are transient and convection effects respectively. The first term on the right hand side represents the gas-flow pressure, the gravity component normal to the surface, and the surface tension. The second term includes the gravity effects parallel to the film. The third and fourth terms represents the viscous shear force at the interface with the gas and within the film respectively. The last term is droplet collection or separation.

In case of thermal modeling the conservation of film energy is also needed:

$$\frac{\partial (HT_f)}{\partial t} + \nabla_s \cdot (\vec{V}_f HT_f) = \frac{1}{\rho C_P} \left[ 2k_f \left[ \frac{T_s + T_w}{H} - \frac{2T_f}{H} \right] + \dot{q}_{imp} + \dot{m}_{vap} L(T_s) \right] \quad (2.37)$$

where  $T_s$  is the surface temperature of the film,  $T_f$  is the average film temperature,  $T_w$  is the wall temperature.  $\dot{q}_{imp}$  is the source term due to droplet impingement to the film,  $\dot{m}_{vap}$  is the rate of mass condensation or vaporization and  $L$  is the latent heat associated with the phase change.[24]

Note that this is not a multiphase model and should therefore be used when the volume fraction of the dispersed phase is negligible in the bulk flow. In ANSYS Fluent it is possible to define species so that the water content of the ventilated air is included, and this is the most efficient way to model moisture transport for a cold attic since the condensation of water takes place at the walls.

### 2.9.4 The VTT model for mold growth

The VTT model [28] is based on laboratory work and comprehensive decay models for mold growth in both constant and fluctuating temperature and humidity conditions. It is a purely mathematical model which is quantified by a mold growth potential, see Table 2.3

**Table 2.3:** Mold growth index for experiments and modeling

Index	Growth rate	Description
0	No growth	Spores not activated
1	microscopic amounts of mould on surface	Growth initialization
2	< 10% of surface covered by mould	Growth initialization
3	10 – 20% of surface covered by mould	Spores produced
4	30 – 70% of surface covered by mould	Moderate growth
5	> 70% of surface covered by mould	Rapid growth
6	Coverage around 100%	Very heavy and dense growth

Experiments on pine and spruce sapwood yielded a polynomial function [28] for the critical humidity level which is being used for the hygrothermal analysis of this study:

$$RH_{crit} = \begin{cases} 100\% & T \leq 0^\circ C \\ -0.00267T^3 + 0.16T^2 - 3.13T + 100 & 0^\circ C \leq T \leq 20^\circ C \\ 80\% & T > 20^\circ C \end{cases} \quad (2.38)$$

The critical level of relative humidity can then be used to calculate the mold growth potential,  $m$ :

$$m = \frac{RH}{RH_{crit}} \quad (2.39)$$

where  $RH$  is the actual (measured) relative humidity at the location of interest and  $RH_{crit}$  is the critical level estimated in equation 2.38.

## 2.10 Radiative heat transfer in Fluent

For the radiative heat transfer, the P-1 model [24] was used. The equations below describes the modeled radiant heat flux,  $q_r$ , for gray radiation:

$$q_r = -\frac{1}{3(a + \sigma_s) - C\sigma_s} \nabla G \quad (2.40)$$

In this equation,  $a$  is the absorption coefficient,  $\sigma_s$  is the scattering coefficient,  $C$  is the linear-anisotropic phase function coefficient and  $G$  is the incident radiation. After introducing the parameter

$$\Gamma = \frac{1}{3(a + \sigma_s) - C\sigma_s} \quad (2.41)$$

the transport equation for  $G$  reads:

$$\nabla \cdot (\Gamma \nabla G) - aG + 4a\sigma T^4 = S_G \quad (2.42)$$

where  $\sigma$  is the Stefan-Boltzmann constant.

## 2.11 Boundary Conditions

For the heat transfer in the attic model, two different kinds of thermal boundary conditions were used. The first one, *Dirichlet*, prescribes a constant or varying temperature at the boundary:

$$T = T_w \quad (2.43)$$

and the second one, *Neumann*, prescribes the heat flux at the wall:

$$k_m \frac{\partial T}{\partial n} = -q_w \quad (2.44)$$

where  $n$  denotes the normal to the boundary and the subscript  $w$  denotes wall. An adiabatic boundary condition where there is no heat flux corresponds to a perfectly insulated wall boundary.

### 3 Method

In this chapter the method used for building the virtual model of the attic and setting up the simulations is presented.

#### 3.1 Software

The Commercial software Icem (ANSYS ICEM CFD) has been used to build the virtual model of the cold attic. It is a software used to build geometries and computational grids for export to a large number of CFD solvers.

The solver that has been used in this project is Fluent (ANSYS Fluent) which is a commercial software containing broad physical modeling capabilities to model single and multiphase flow, turbulence, heat transfer and reactions. This software is well known and widely used for CFD applications.

To prepare transient tables for time-dependent boundary conditions, and to prepare hand calculations and post-processing MATLAB has been used.

#### 3.2 Geometry

The virtual model represents the upper part of a residential house including a layer of insulation with an overlying air cavity. This model was constructed according to the dimensions used in [13, 15, 16] with a few modifications which are explained in this chapter. These dimensions are, in turn, taken from common values for cold attics [30, 31]. In order to minimize the computational time of the simulations, the model was built to represent only a section of an actual attic construction, with the assumption that symmetric behavior of the flow pattern is present in the direction parallel to the sidewalls. This will be discussed further in section 3.4.2.

The ventilation system is designed with one inlet positioned in a gap between the end of the roof and the insulation and an outlet in the corresponding gap at the opposite side of the attic. As the air enters the attic it is guided through a passage between the roof and the wind deflectors which prevent the incoming air from flowing directly into the insulation. In the previous research, [13, 15, 16], the so called ridge ventilation system [32, 33] was used whereupon the outlet was positioned at the top of the roof. It was seen that the ventilated air tended to follow the roof boundary directly from the inlets to the outlet without any clear interaction with the rest of the domain which is why a different type of ventilation system is implemented for this research.

In figure 3.1 and table 3.1 an overview of the attic with description of the boundaries are presented. A cross section of the attic model is shown in figure 3.2 where the dimensions are given as well as a visualization of the boundary conditions. The temperatures,  $T_{amb}$ ,  $T_{eq}$  and  $T_{hot}$  in the lower picture of figure 3.2 are explained in section 3.4.2. The depth of the attic is 1800 mm and the insulation is 400 mm at the thickest section.

At the floor boundary within the insulation lies wooden joists perpendicular to the side walls that stretch from one wall to the other. These wooden joists have a relatively high conductivity compared to their environment and their presence has a significant impact on the heat transfer process and the flow pattern in the insulation [34]. The placement of the joists is shown in figure 3.3. The joists are 135 mm high and 45 mm thick, and they are placed with a 600 mm spacing between the centers of each joist. Normally there are joists along the roof boundary as well but in this model they are not included. Instead, the heat capacity of the system was increased by adding additional density,  $\Delta\rho$ , to the insulation to account for

fictive joists in the roof. As explained in section 3.4.1, the insulation is modeled as a porous zone and an increase in density does therefore not affect the flow within it.

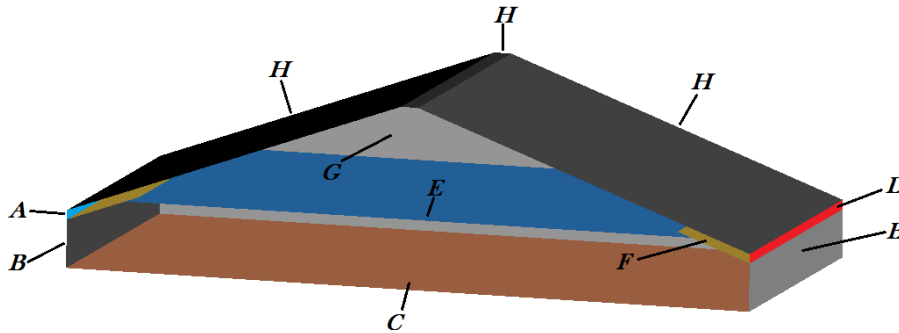


**Figure 3.1:** Overview of the Attic Model.

**Table 3.1:** Explanation of Figure 3.1

A	Inlet
B	Side Walls
C	Floor
D	Outlet
E	Top surface of Insulation
F	Wind deflectors
G	Front/back walls
H	Roof

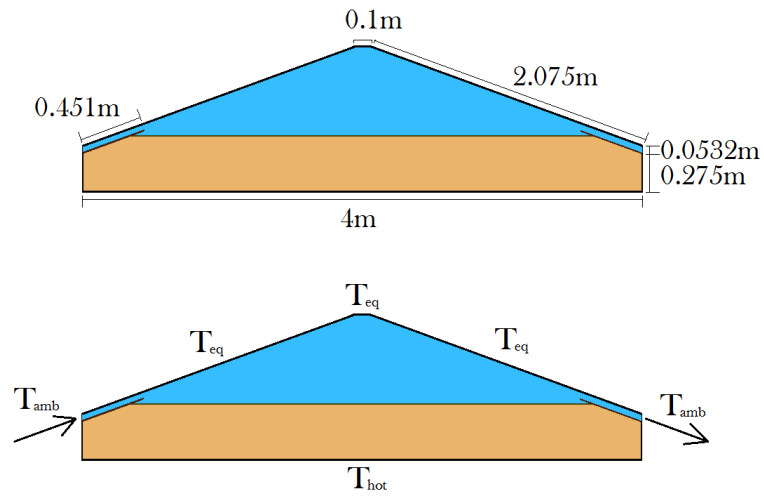


**Figure 3.2:** Cross section of the Attic Model. The upper picture shows the outer dimensions of the model and the lower one gives the flow direction and boundary conditions. The lower region represents the insulation layer and the upper on the air cavity.

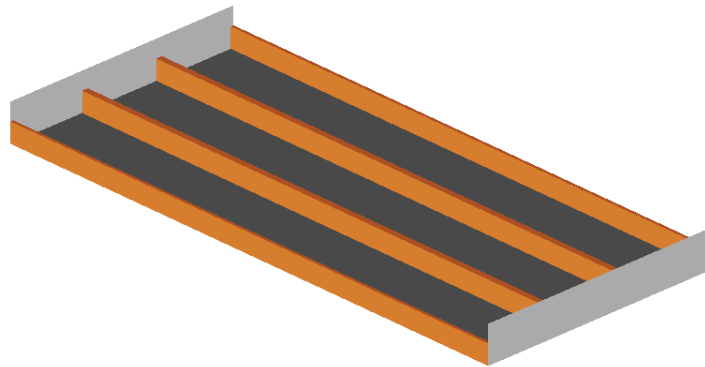


**Figure 3.3:** Placement of the joists in the insulation.

### 3.3 Mesh

Icem was used to build a structured volume mesh containing only hexahedral cells. Once the geometry is defined, several blocks are defined to help constructing the mesh and controlling its density in different regions. By using this method, the user has full control of the distribution of the cells and in many cases the structured mesh has better quality than the unstructured one.

### 3.3.1 Mesh Independence Study

According to agreements between Chalmers University of Technology and ANSYS, The maximum number of computational cells is 512000 for use of the academic license provided for educational purposes. If a larger mesh is used one has to use a research license which is normally not available for thesis projects. Due to this constraint, the mesh was built with caution to distribute the cells efficiently in the domain. Despite these restrictions, a mesh independence study was performed by temporary use of a research license, for several mesh sizes in order to investigate the validity of the mesh. The results can be seen in figure 3.4 where the scaled residuals of continuity, Energy and P1-radiation are plotted for different mesh sizes.

The smallest mesh was built containing approximately  $148 \cdot 10^3$  computational cells and the settings of the simulation were set as explained in Section 3.4 so that a converged solution could be obtained. Initially with the default settings in Fluent the simulations suffered from extremely high continuity residuals, which was also noticed in [13, 14, 15, 16], and this problem was solved mainly by a proper choice of spatial discretization. As a converged solution was obtained according to convergence criteria recommended by fluent (See Table 3.2), the final values of the residuals as well as temperatures in three monitor points in the domain were stored. The mesh size was then globally increased with a factor of 1.5 and the same data was monitored for the larger mesh as the simulations ran. This procedure was then repeated up to a mesh size of  $1125 \cdot 10^3$  computational cells. The stored data from the simulations was then plotted as functions of mesh size, but due to the nature of heat transfer problems with natural convection the temperatures in the monitor points did vary even though the residuals were low and stable. This made it difficult to draw any conclusions by viewing the temperatures, so instead the dependency of the mesh size was investigated for the residuals solely. The results from the mesh independence study showed that the solution becomes independent of mesh size for mesh sizes equal to, or larger than approximately 500000 cells. Only three of the residuals are presented in Figure 3.4 to make it easier to overview. Continuity was chosen because it always had the highest value, and Energy and P1 was included because they have a stricter convergence criteria.

Pictures of the final mesh can be seen in figure 3.5 and 3.6.

**Table 3.2:** Convergence criteria for residual levels

Continuity	$10^{-3}$
X-velocity	$10^{-3}$
Y-velocity	$10^{-3}$
Z-velocity	$10^{-3}$
Energy	$10^{-6}$
$k$	$10^{-3}$
$\varepsilon$	$10^{-3}$
P1	$10^{-6}$

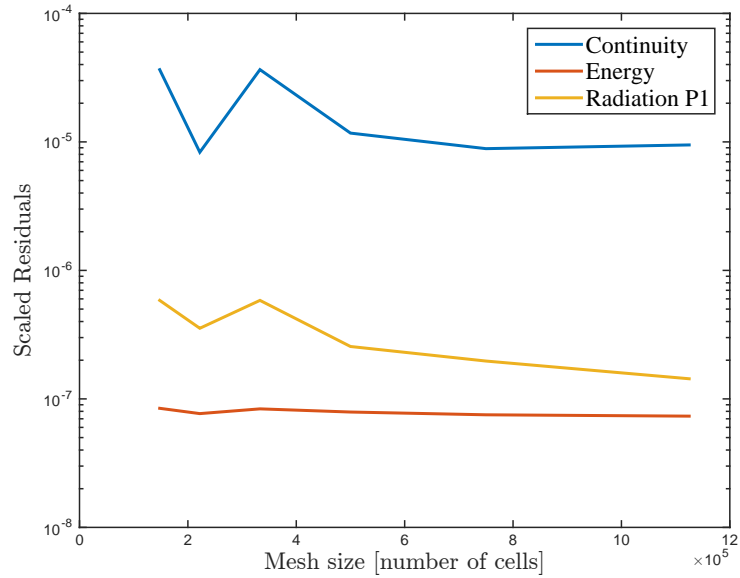


**Figure 3.4:** Scaled residuals of continuity, Energy, and P1 radiation obtained after converged solutions. Mesh sizes ranging from  $148 \cdot 10^3$  to  $1125 \cdot 10^3$  cells

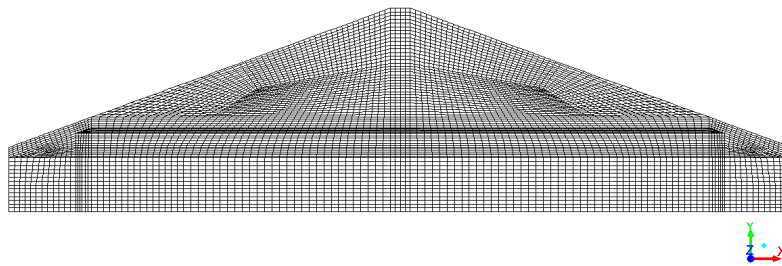


**Figure 3.5:** The attic model mesh viewed in the xy-plane

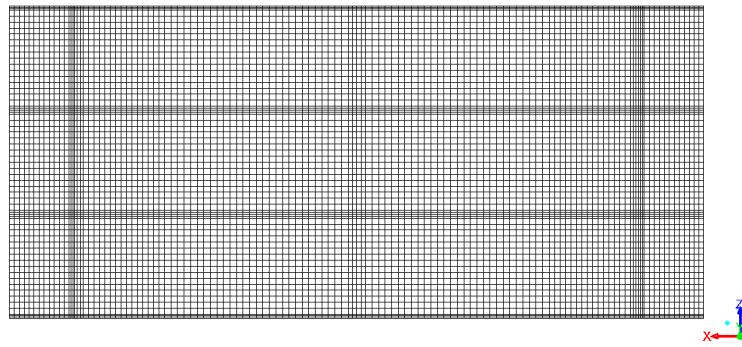


**Figure 3.6:** The attic model mesh viewed in the xz-plane

### 3.4 Fluent Settings

In this section, the settings in fluent are presented. There are many adjustments that can be made in commercial CFD software, and small modifications in the settings can have a large impact on convergence as well as the results. During the beginning of this project a lot of focus was put into modifying the settings in order to get a converged solution with residuals at acceptable levels. The level of convergence showed to be very sensitive and highly dependent on the choice of numerical scheme for pressure-velocity coupling, the spatial discretization method and the under-relaxation factors. In Table 3.3 the most relevant settings for running the simulations are presented. Table 3.4 gives the chosen methods for spatial discretization, and under-relaxation factors are presented in Table 3.5.

**Table 3.3:** General Fluent Settings

Time Dependency	Transient
Solver Type	Pressure-Based
Turbulence Model	Realizable $k - \varepsilon$ model
Wall Function	Standard
Radiation Model	P1
Pressure-Velocity Scheme	SIMPLE
Time Stepping Method	Fixed

**Table 3.4:** Spatial Discretization Methods

Gradient	Green-Gauss Node Based
Pressure	Body Force Weighted
Momentum	Power Law
$k$	Power Law
$\varepsilon$	First Order Upwind
Energy	Power Law

**Table 3.5:** Under-Relaxation Factors

Pressure	0.3
Density	0.9
Body Forces	0.9
Momentum	0.1
$k$	0.8
$\varepsilon$	0.8
Turbulent Viscosity	0.9
Energy	0.9
P1	0.5

### 3.4.1 Modeling the Insulation

In order to mimic the flow properties of an insulation layer, the volume containing the insulation is defined as a porous zone in Fluent. This means that there is no actual material added in this region. Instead, resistance coefficients and the thermal conductivity are changed by modifications of the fluid properties and by addition of an extra source term in the momentum equation, as explained in Section 2.8.3.

By defining a porous zone in Fluent, resistances for conductive and convective heat transfer are introduced for the particular zone. It is, however, not possible to include any resistance for the radiative heat transfer within the insulation in the current version of Fluent which results in an over prediction of the heat flow within the porous zone. This is simply because the volume is modeled as a without any matter that absorbs or emits radiative energy, See Section 2.7.3. There are ways to mimic the effects of radiative resistance by running multiple simulations for the same case by first solving the temperature field with the insulation defined as a solid and then solving the flow field with the volume defined as a porous zone. There are also other commercial CFD softwares that are able to model radiative resistances for porous zones, but it is out of the scope for this project to investigate other possibilities.

The velocities within the insulation volume is assumed to be very low, and the porous zone was therefore defined as a so called laminar zone in Fluent. This is a common approximation for insulated volumes and is a recommended setting by [25] as long as the permeability is not too large. Inclusion of turbulence in the porous zone was also tested in the previous thesis project [13, 14] where it showed to give unphysical solutions.

In [14], the CFD model was validated by comparison with experiments performed by Serkjitis [17]. Two different permeabilities,  $4 \cdot 10^{-8} \text{ m}^2$  and  $5 \cdot 10^{-8} \text{ m}^2$ , were used for the porous zone and in this thesis the higher value has been used. The thermal conductivity of the insulation material was set to a constant value of  $0.044 \text{ W}/(\text{m} \cdot \text{K})$  which is not completely physical but this approximation was made due to small changes in temperature of the insulation for different roof temperatures. This is the same conductivity as in the experiments that the model was validated with in [14].

### 3.4.2 Boundary Conditions

As mentioned in Section 3.2, only part of the model is being simulated in order to minimize the computational intensity of the simulations. At the front and back walls (See Figure 3.1 and Table 3.1) a symmetry boundary conditions was set to account for the excluded parts of the attic.

For the side walls, Neumann boundary conditions were set with a prescribed temperature gradient

of zero. This choice is based on an approximation made in [14], where it was found that a Neumann boundary condition at these walls helped getting faster convergence compared to the more intuitive choice of a Dirichlet boundary condition with a prescribed outdoor temperature, and that the difference between the two was rather small.

The inlet was set to prescribed constant velocities defined in vector components to direct the flow parallel to the roof and the wind deflectors. Three different velocities, 0.0226 m/s, 0.0452 m/s and 0.0904 m/s, were set which correspond to 2, 4 and 8 complete air displacements per hour, respectively. A pressure outlet with Atmospheric pressure was set for the outlet.

Common for the inlet and outlet was the Dirichlet temperature boundary condition which was set to a time dependent ambient air temperature,  $T_{amb}(t)$ . In the same way the roof boundary was set to the equivalent temperature,  $T_{eq}(t)$ , defined in Section 2.4. Data files with hourly measured temperature levels were analyzed and processed in MATLAB, and ambient and equivalent temperatures were exported as transient tables to Fluent. These files contain time dependent temperature levels for a 24-hour cycle in the middle of April. These Dirichlet boundary conditions are visualized in Figure 3.7. At the floor a Dirichlet boundary condition was set with a prescribed temperature,  $T_{hot}$ , of 294 K which was kept constant for all cases. The wind deflectors were defined as shell conduction elements, with plywood as material and a fictive thickness of 10 mm, to allow conduction through them. The roof boundary was also defined as plywood but with a fictive thickness of 22 mm. All boundary conditions are summarized in Table 3.6.

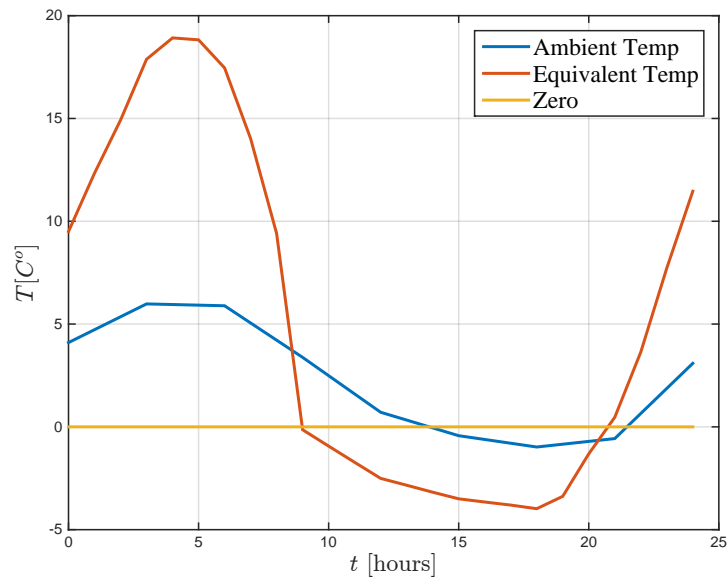


**Figure 3.7:** Plot of ambient and equivalent temperatures along with a line showing the zero point

**Table 3.6:** Attic Model Boundary Conditions

Inlet	Velocity Inlet, $u = 0.0226 - 0.0904$ m/s, $T = T_{amb}(t)$ K
Outlet	Pressure Outlet, $P =$ Atmospheric Pressure, $T = T_{amb}(t)$ K
Roof	Dirichlet, $T = T_{eq}(t)$ K
Floor	Dirichlet, $T = 294$ K
Side Walls	Neumann, $dT/dx = 0$
Back/Front Walls	Symmetry
Wind Deflectors	Shell Conduction

### 3.5 Running the Simulations

The simulations were ran with the Academic license for ANSYS Fluent on a local machine at Chalmers University of Technology.

For the transient simulations a fixed time step of 1 s was used, which is an extremely large time step. It was, however, found that the solution was almost steady even though the temperature boundary conditions for inlet, outlet and roof are varying with time, which made it possible to use such large time steps without slow convergence. The simulations were first initialized for a number of time steps with constant Dirichlet boundary conditions to ensure that the temperatures and velocities in the domain had settled before the actual 24-hour cycle was simulated. These boundary conditions were the same as the start value for the transient boundary conditions.

The convergence criteria was defined as in Table 3.2 and the residuals were monitored as the simulations ran. A number of monitor points that were systematically distributed in the domain were also monitored to ensure that the results were reasonable.

At 5 locations along the roof boundary (red circles in Figure 3.8) the temperatures at the inner roof was monitored to give input for the hygrothermal analysis. These locations are marked with red circles in Figure 3.8.

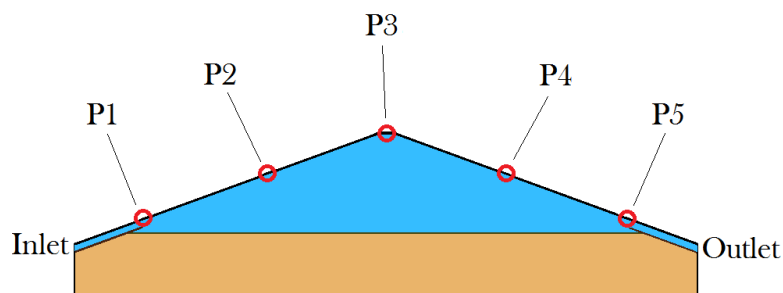


**Figure 3.8:** Cross section of the attic model showing the location of the 5 monitor points along the inner roof boundary. Each red mark represents two points in the direction normal to the cross section, one above the center of a joist and one in the middle between two joists.

For the second part of this study the Eulerian Wall Film Model was activated for the inlet-side of the roof. The simulations were initiated with a film of water with a thickness of 0.5 mm to simulate

drying of a wall that is already wet. Four different ventilation rates, namely 2, 4, 6 and 8 complete air displacements per hour, were investigated to see how the thickness of the film was varying for different Reynolds numbers. For these simulations the thermal boundary conditions of the roof and the ambient air were taken as the values that correspond to the coldest part of the 24-hour cycle. Despite the fact that the external conditions were constant the simulations were solved as transient since the wall film model is a time dependent model. The time step for the bulk flow was kept as 1 s while the time step of the Eulerian Wall Film Model was set to 0.2 s.

## 4 Results

The results of this thesis project are mainly presented in paper 1 and paper 2, which are attached in the appendix of this report. This chapter summarizes the results of each paper. The color bars in the figures with temperature contours are divided in 20 nuances where each step in color represents approximately 1 K. For the contours of water mass fraction and wall film thickness the increments in nuance of the color bar represent approximately  $0.065 \text{ g}_{\text{water}}/\text{kg}_{\text{air}}$  and 0.06 mm respectively.

### 4.1 Paper 1: Transient Heat Transfer and Moisture Load in Cold Attic Constructions - A CFD Analysis

The calculated Nusselt number for the insulation as a function of time is presented in figure 4.1 where the three lines represent different ventilation rates. The four crosses that are plotted in the figure are values of the Nusselt number that correspond to the experimental results [17].

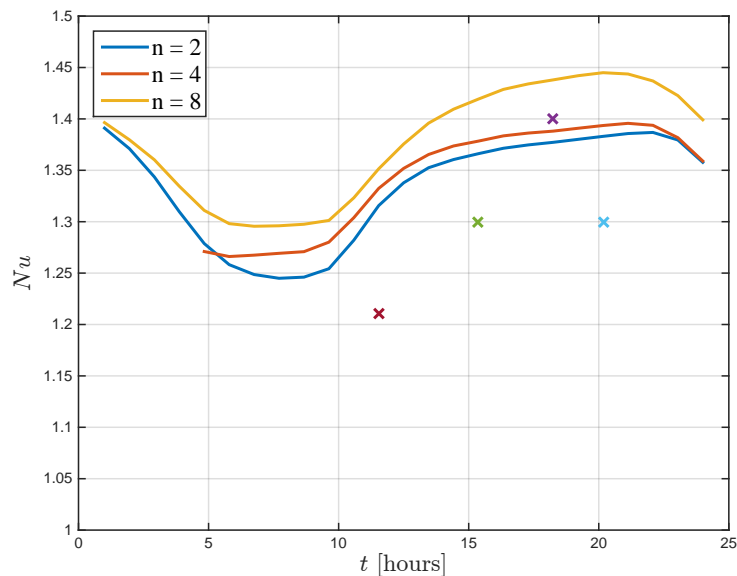


**Figure 4.1:** Nusselt number versus time in the insulation layer calculated each hour for all ventilation rates.  $n=2$ ,  $n=4$  and  $n=8$  denotes 2, 4 and 8 complete air displacements per hour respectively. The four crosses show values obtained from experiments with pure natural convection [17]

Temperature contours for a plane in the middle of the domain are found in figure 4.2. This figure shows the temperature profiles at the coldest point of the 24-hour cycle for the three different ventilation rates.

The information needed to calculate the mold growth potential is the temperature at the inner surface of the roof and the humidity levels. The levels of humidity by volume, presented in Figure 2.1 in Chapter 2, are given as one hourly updated sample of measured data and one constant level which represents the whole month of April. The temperatures at the inner roof, calculated in the CFD-simulations, are presented in Figure 4.3.

As concluded by looking at Figure 4.2 the temperature levels varies along the inner roof boundary, so to give more specific results for different parts of the roof the inner roof temperatures were also calculated

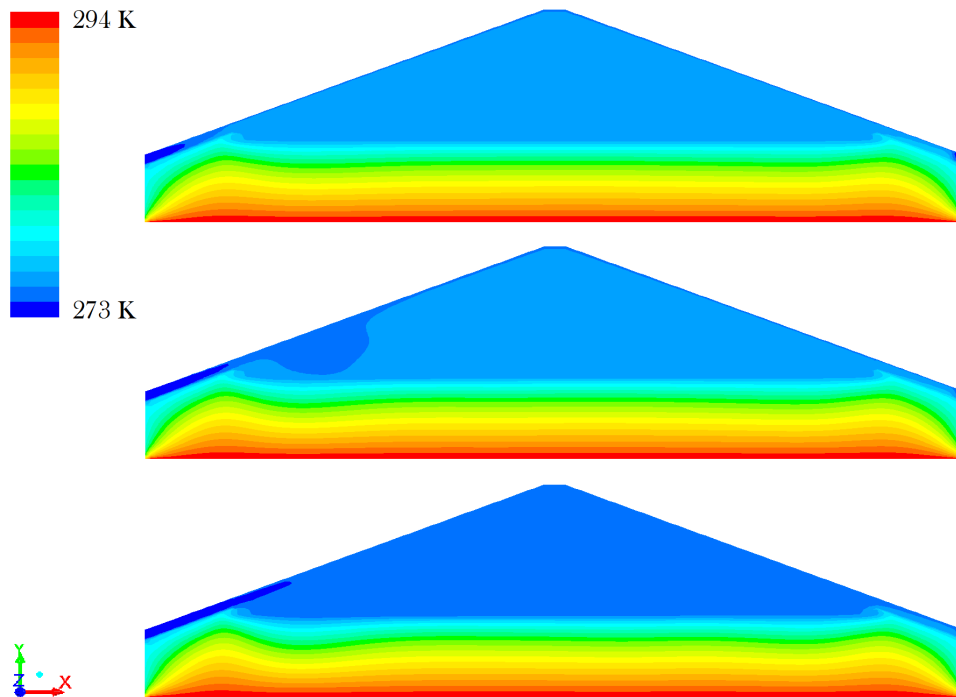


**Figure 4.2:** Temperature contours for the middle of the night when the temperature difference is largest, taken in the  $xy$ -plane in the middle of the attic. The plots are for, in order from above, 2, 4 and 8 complete air displacements per hour.

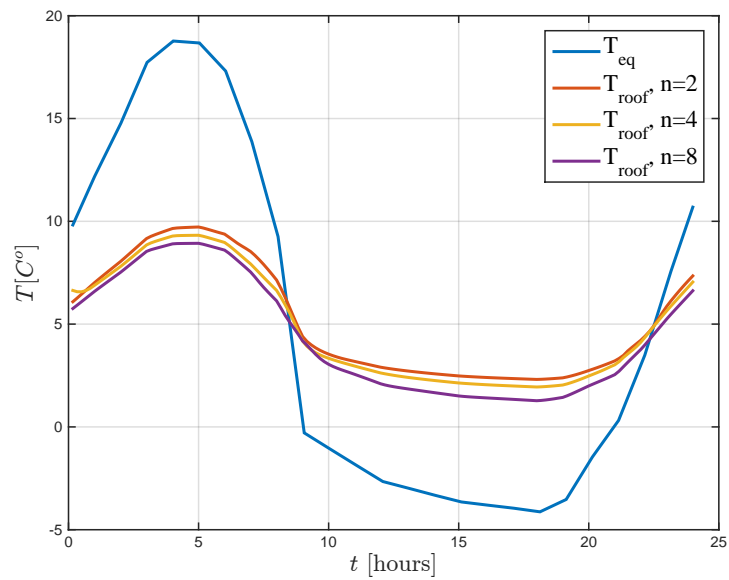


**Figure 4.3:** The boundary condition for the roof boundary,  $T_{eq}$ , versus time, plotted along with the mean inner roof temperature for the three ventilation rates.

at the locations shown in Figure. 3.8 in the end of the previous chapter. The level of relative humidity and the mold growth potential were calculated with Equations 2.9-2.13 and 2.38-2.39 with the two different humidity inputs and the results are presented in Figure 4.4 to 4.13.

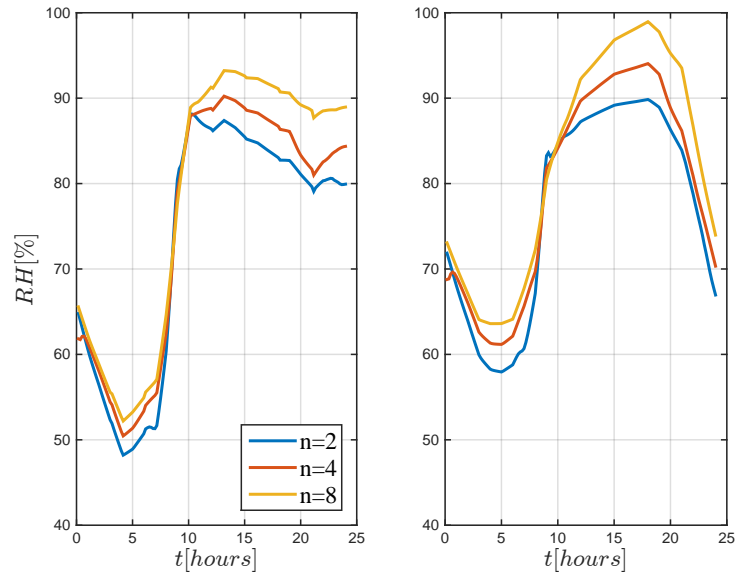


**Figure 4.4:** Relative humidity versus time measured at location P1 (see fig. 3.8). The left plot shows the values calculated from the time dependent  $v_e$  and the right plot shows values from the averaged one, and the same goes for fig. 4.5, 4.6, 4.7 and 4.8.

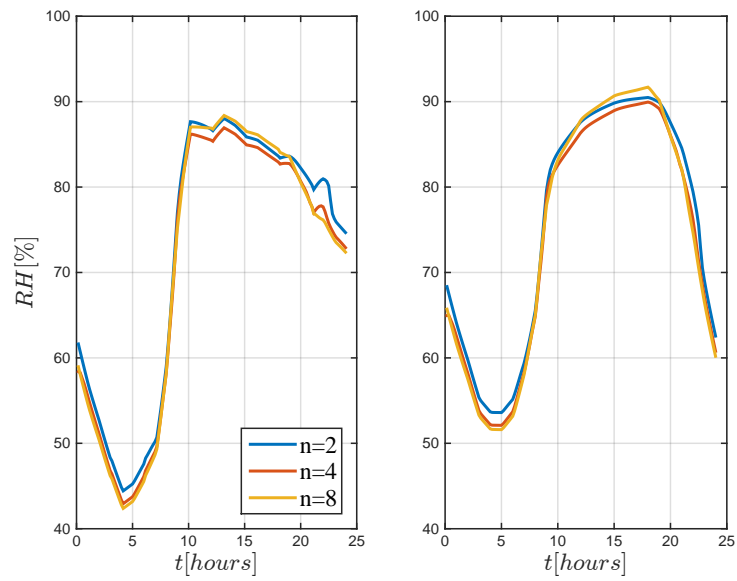


**Figure 4.5:** Relative humidity versus time measured at location P2.

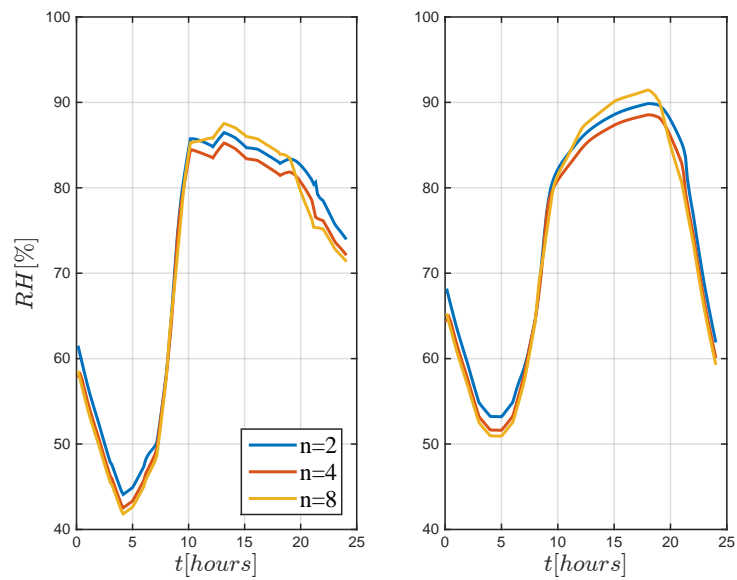


**Figure 4.6:** Relative humidity versus time measured at location P3.

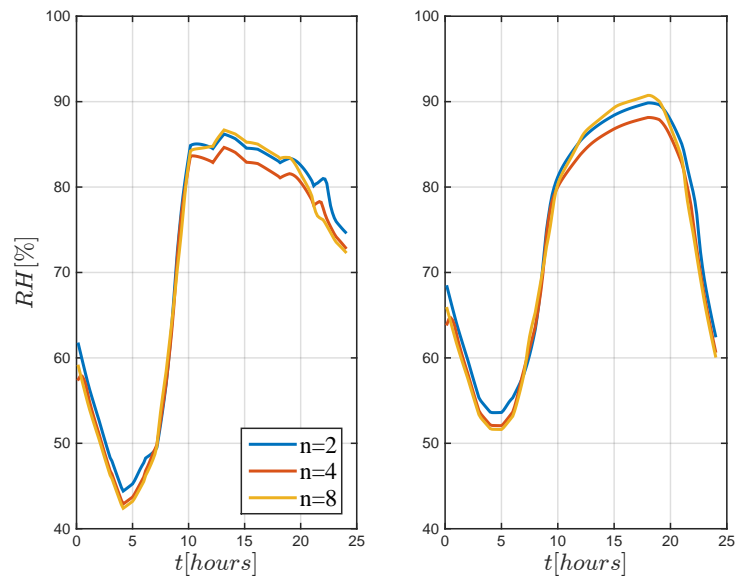


**Figure 4.7:** Relative humidity versus time measured at location P4.

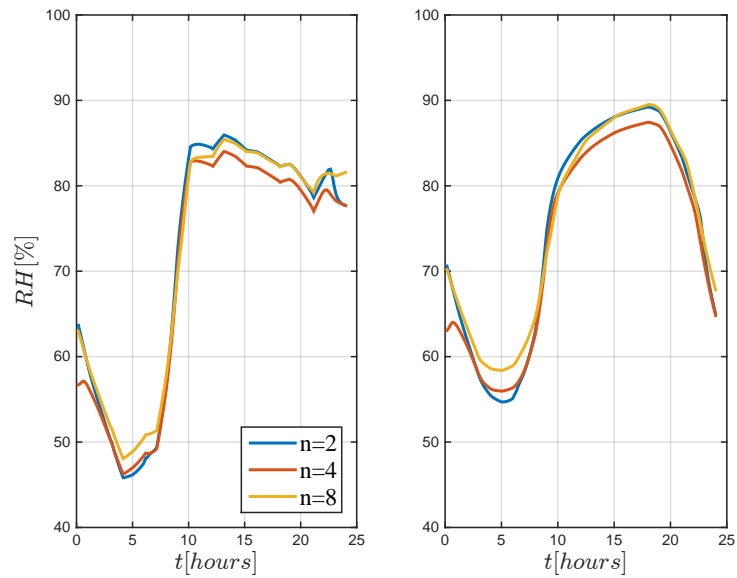


**Figure 4.8:** Relative humidity versus time measured at location P5.

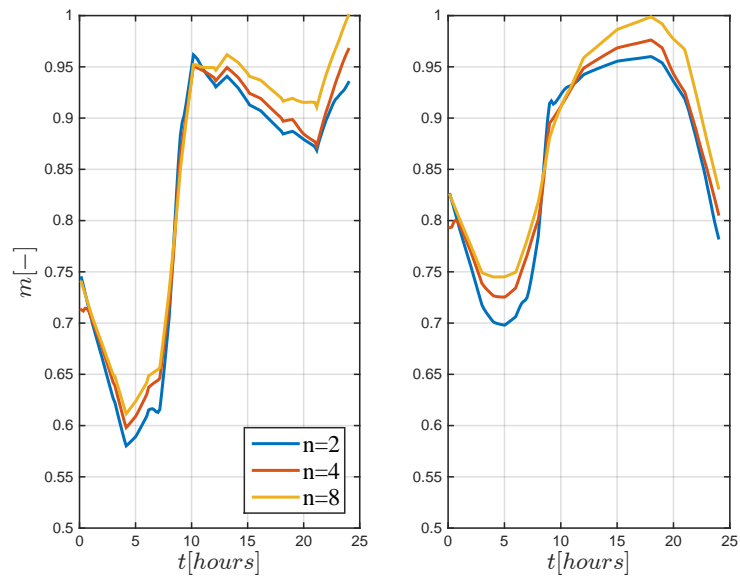


**Figure 4.9:** Mold growth potential,  $m$ , versus time measured at location P1 (see fig. 3.8). The left plot shows the values calculated from the time dependent  $v_e$  and the right plot shows values from the averaged one, and the same goes for fig. 4.10, 4.11, 4.12 and 4.13.

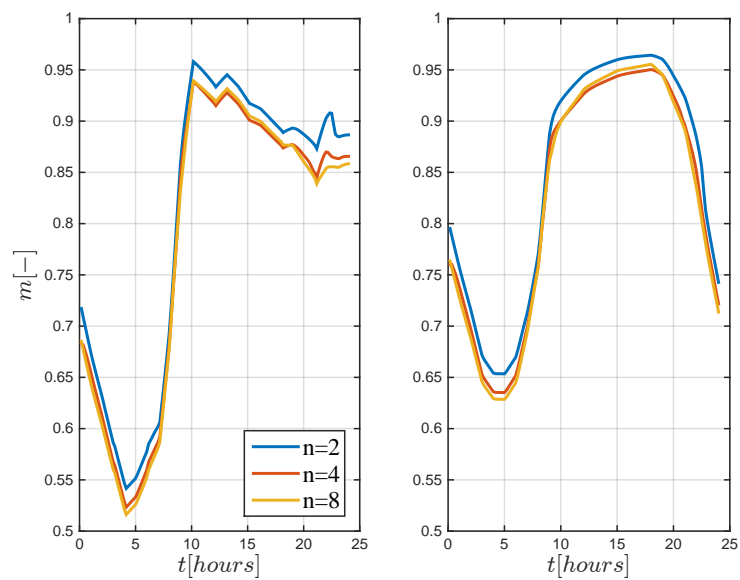


**Figure 4.10:** Mold growth potential,  $m$ , versus time measured at location P2.

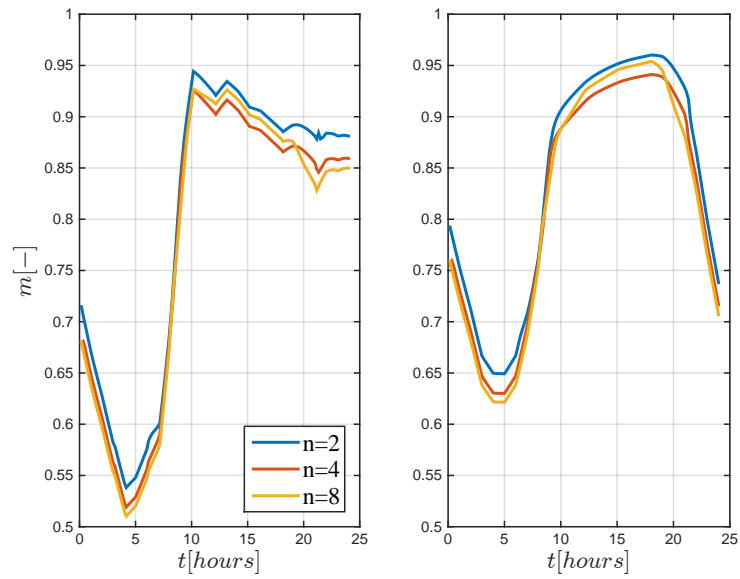


**Figure 4.11:** Mold growth potential,  $m$ , versus time measured at location P3.

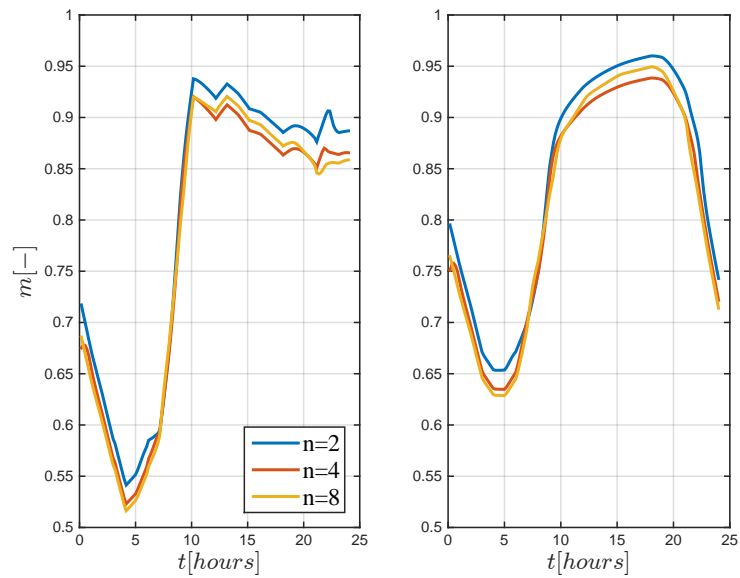


**Figure 4.12:** Mold growth potential,  $m$ , versus time measured at location P4.

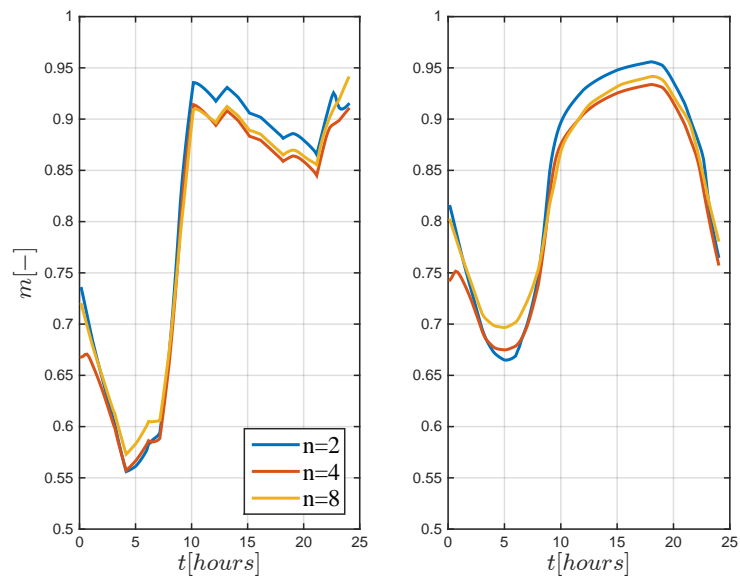


**Figure 4.13:** Mold growth potential,  $m$ , versus time measured at location P5.

## 4.2 Paper 2: Transient Modeling of Heat Transfer and Evaporation in Cold Attics - A CFD Analysis

The simulations with the Eulerian Wall Film model were executed with constant thermal boundary conditions corresponding to the outdoor climate at the coldest part of the 24-hour cycle that was studied in paper 1. 4 different ventilation rates were investigated. The wall film was activated at the inner surface of the inlet-side of the roof since this was found in paper 1 to be the most critical part of the roof boundary. The results presented in this section are meant to show the ability of the ventilated air to dry a surface that is already wet. Temperature contours for the middle plane of the domain can be found in figure 4.14. The contours in the figures shows results for different ventilation rates after 20000 time steps, which equals 5.5 hrs.

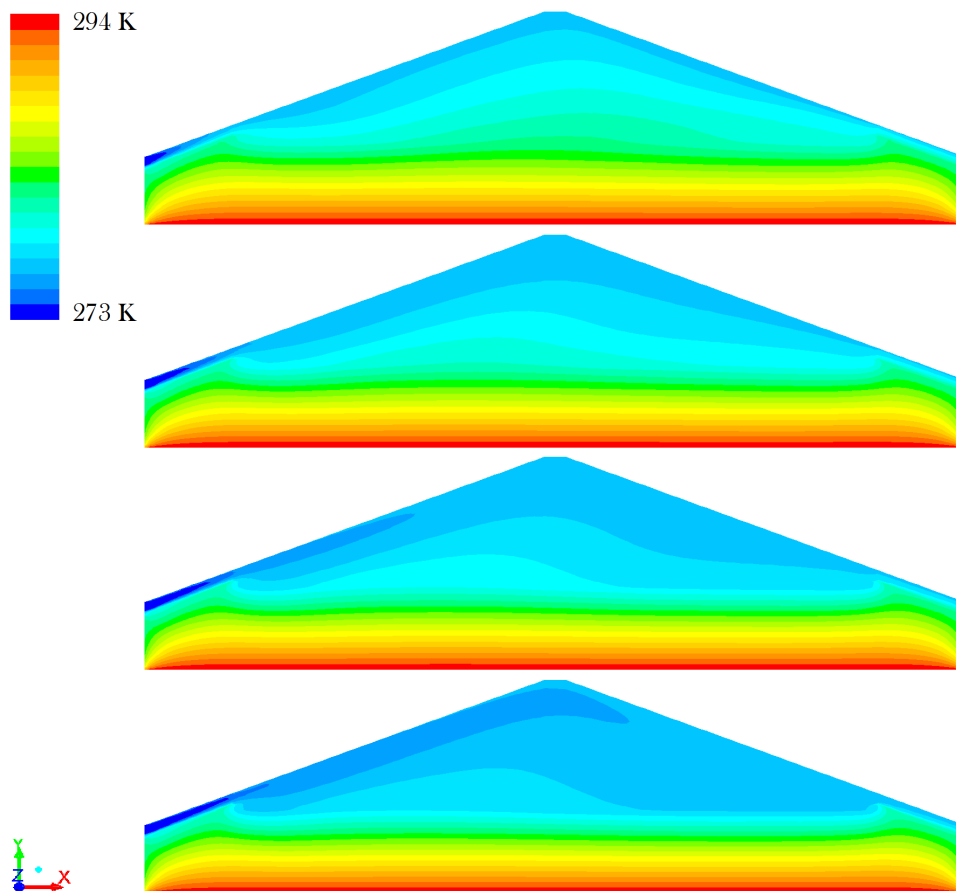


**Figure 4.14:** Temperature contours in a cross section in the middle of the attic for different ventilation rates. The pictures represent, from above, 2, 4, 6 and 8 complete air displacements per hour respectively.

The mass fraction of water in the middle cross section plane of the domain is shown in Figure 4.15. For the lower ventilation rates a region of higher water concentration is found close to the wall film boundary and as the ventilation rate increases the ventilated air has a greater potential to dry out the wall.

Contours of the water film thickness is presented in top views of the inlet-side of the roof in Figure 4.16. The left edge of the plots is the lower edge of the roof where the inlet is positioned and the right edge is

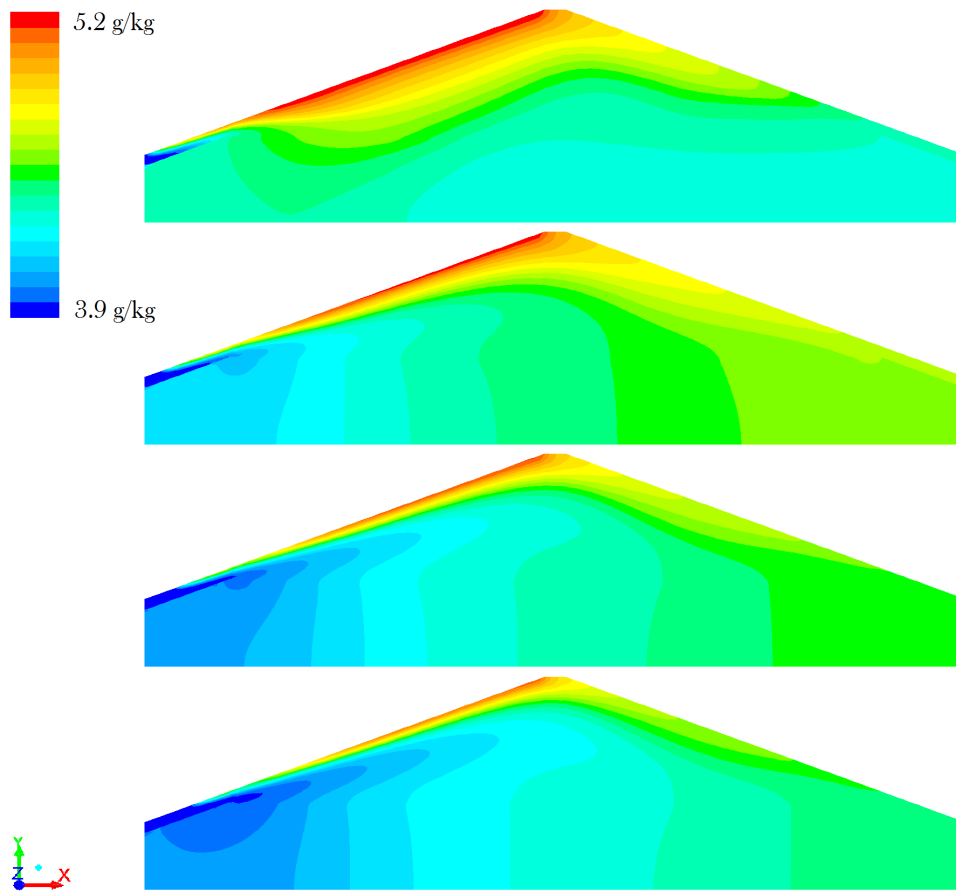


**Figure 4.15:** Contours of mass fraction of water [ $\text{g}_{\text{water}}/\text{kg}_{\text{air}}$ ] in a cross section in the middle of the attic for different ventilation rates. The pictures represent, from above, 2, 4, 6 and 8 complete air displacements per hour respectively.

the top of the roof. There is a clear difference in film thickness and also in the distribution of the water at the surface for different ventilation rates.

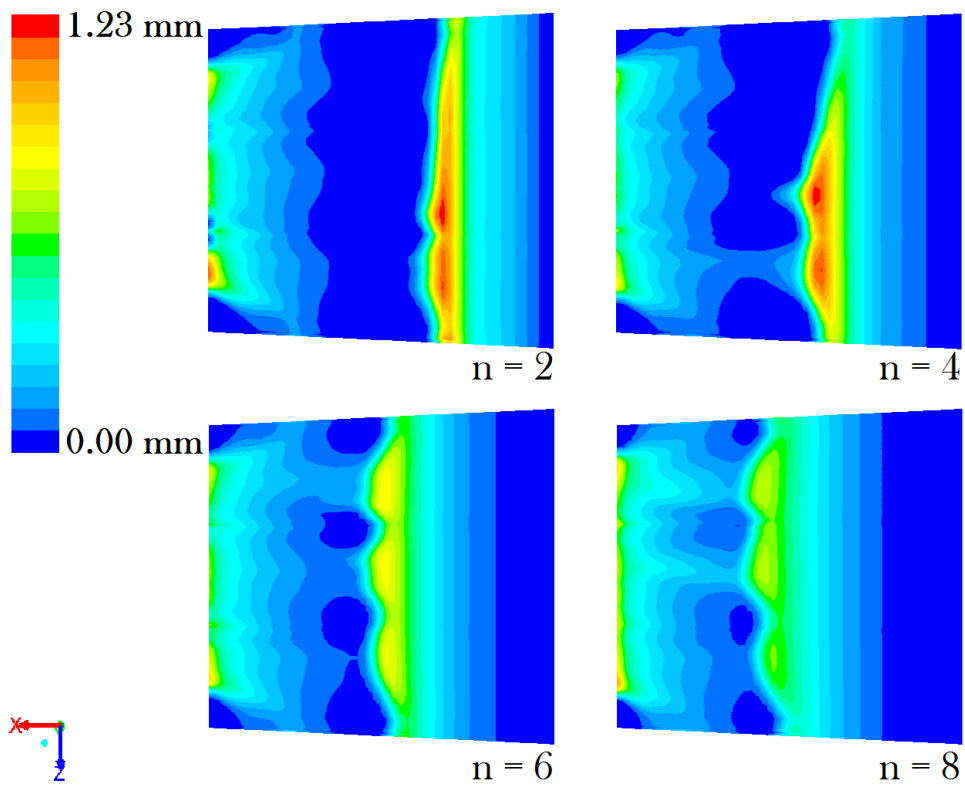


**Figure 4.16:** Contours of Eulerian Wall Film thickness plotted at the roof of the attic closest to the inlet for different ventilation rates. The right edge of each figure is the edge where the inlet and the roof meet, and the left edge of each figure is the top of the roof. The pictures represent, from above, 2, 4, 6 and 8 complete air displacements per hour respectively.

## 5 Discussion and Conclusions

The results of the research work presented in paper 1 and 2 shows that the CFD-model used in this project gives results that are physical and they agree well with findings from previous research. As mentioned in the report, this is a continuation of a previous Master's Thesis project [13, 14, 15, 16] where high residuals of continuity was a problem that was left unsolved. There was a lot of time spent in the beginning of this project in order to get better convergence and with the right choice of spatial discretization and under-relaxation factors the solution was successfully able to fulfill the convergence criteria recommended by fluent. It should be mentioned that running transient simulations also helped achieving better convergence for this problem.

ANSYS Fluent has shown to be a robust CFD software for solving heat transfer problems involving natural and forced convection. It is, however, of interest for future research to investigate advantages and disadvantages with other commercial software. This is mainly due to the fact that the only way of modeling the properties of insulation material is to define the region of interest as a porous zone, which in Fluent implies that the region is treated as a fluid with modified source terms for momentum. This eliminates the possibilities to account for resistance to radiative heat transfer in the porous zone since that would require presence of matter. The way porous zones are modeled in Fluent leads to an over prediction in radiative heat transfer and, for this reason, possibilities with other software should be investigated.

The modifications that has been made in the geometry of the model that was used in the previous thesis [13, 15, 16], have shown that the inlet-outlet configuration has a significant impact on the heat transfer rate in the air cavity as well as the insulation. As the wind deflectors were shortened the ventilated air was more likely to separate from the roof boundary and cool down the top of the insulation layer which amplifies the convective heat transfer. This shows that the convective heat transfer is more dominant in the geometry that was used in this project compared to the one used in [13, 16].

Furthermore, it was found that convective heat transfer is always present within the insulation for the chosen 24-hour cycle, and also that the highest ventilation rate gives approximately 5% higher values of the Nusselt number than the lowest. This means that the heat loss from the living area is increased with 5% if the ventilation rate of the attic is increased from 2 to 8 complete air displacements per hour.

The temperature difference over the insulation at four times of the 24-hour cycle were used to calculate the modified Rayleigh number by extrapolation of the results from Serkitjīs study [17]. The values of the Rayleigh number were, in turn, used to get values of the Nusselt number. This was done as a rough comparison with experimental results to see if the calculated values were reasonable. The study by Serkitjīs was performed for pure natural convection without any joists which explains the difference in the results but it shows that the values of the Nusselt number obtained from this study are reasonable. Since there are no previous experiments performed for attics with the climatic conditions applied in this study, the validity of the model relies on the validation performed in the previous Master's thesis project [14].

From the hygrothermal analysis it is concluded that the lower part of the roof at the inlet-side is the most critical region. In this region the mold growth potential reaches a value of 1 for the coldest part of the night. This is also the region where the greatest dependency on the ventilation rate is found, where the highest ventilation rate gives the greatest risk for microbial growth.

Regarding EWFM, the results should be interpreted as drying effects of ventilated air with different speeds on a water film at a blank surface that is already wet. At this stage, the study about condensation doesn't bring much valuable information about the physical phenomena in cold attics since the exact situation that was investigated is rare for buildings. A more accurate way to go would be to model absorption of water at the roof boundary - something that didn't fit in the scope of this study.

It is, however, possible to see how the distribution of water is affected by the wind speed. For low speeds, high concentrations of water are found at some locations while some areas of the roof are completely dry. For higher speeds the film thickness is lower but a larger part of the surface is wet. The highest

thicknesses are found at the lower part of the roof boundary, approximately where the wind deflectors end, which is also the part of the roof where the highest mold growth potential was found in paper 1.

## 5.1 Future Work

In this thesis project, tools have been developed in order to model the transient heat transfer and moisture load in a full scale attic model exposed to real climatic conditions measured in Sweden. The steps listed below suggests possible improvements and future applications of the developed model:

- Investigate possibilities of modeling resistance to radiative heat transfer in the insulation. ANSYS Flunet is currently lacking the ability to account for this which leads to an over prediction of the radiative heat transfer. This can be done by using another CFD-solver, or by combining ANSYS Fluent with other software specialized in radiation, such as RadTherm.
- Add wooden joists along the roof boundary since this affects the total heat capacity of the system as well as the flow pattern in the air cavity.
- Identify and apply a suitable model for absorption of water at the inner roof boundary in order to vindicate the implementation of the EWFM.
- Introduce optimization methods, such as Design of Experiments (DOE), in order to optimize the ventilation design, ventilation rate for moisture safety and different attic configurations.

## Bibliography

- [1] American Society of Heating, Refrigerating and Air-Conditioning Engineers. (2013). *2013 ASHRAE handbook: fundamentals*. ASHRAE.
- [2] Hagentoft, C-E. (2002). *Vandrande fukt Strålände värme. så fungerar hus*. Studentlitteratur, Sweden.
- [3] Boverket. (2010) *God bebyggd miljö - förslag till nytt delmål för fukt och mögel, Resultat om byggnaders fuktskador från projektet BETSI*. Karlskrona: Boverket
- [4] Ojanen, T., Viitanen, H., Peuhkuri, R. (2007) *Modelling of Mold Growth*. VTT - Technical Research Centre of Finland.
- [5] Hagentoft, C-E. Sasic Kalagasidis, A. (2010) *Mold Growth Control in Cold Attics through Adaptive Ventilation: Validation by Field Measurements*.
- [6] Hukka, E., H.A. Viitanen. (1999). A mathematical model of mold growth on wooden material. *Wood Science and Technology* 33.
- [7] Shankar, V., Davisson, L., Olsson, E. (1995). *Numerical Investigation of Turbulent Plumes in both Ambient and Stratified Surroundings*, Journal of INDOOR AIR, Denmark.
- [8] Shankar, V., Hagentoft, C-E. (2000). *Numerical Investigation of Natural Convection in Horizontal Porous Media Heated from Below – Comparisons with Experiments*, Journal of Thermal Envelope and Building Science, vol. 23.
- [9] Shankar, V., Hagentoft, C-E. (2000). *A Numerical Study of Effect of Natural Convection on Thermal Properties of Horizontal Oriented Porous Insulation*, Journal of Thermal Envelope and Building Science, vol. 24.
- [10] Shankar, V., Hagentoft, C-E. (1999). *Influence of natural convection on the thermal properties of insulating porous medium with air cavity*. Indoor air 99, Edinburgh.
- [11] Wang, J. (2003) *Heat and Mass Transfer in Built Structures*. Göteborg: Chalmers University of Technology. (Doctoral Thesis, Department of Building Physics)
- [12] Lejon, M., (2013). *Wall Condensation Modeling in Convective Flow*. Stockholm: KTH, Industrial Engineering and Management. (Master's Thesis)
- [13] Bengtson, A., Fransson, V. (2014). *Influence of Natural and Forced Convection in Attics - A CFD Analysis*. Göteborg: Chalmers University of Technology. (Master's Thesis, Department of Civil and Environmental Engineering)
- [14] Shankar, V., Bengtson, A., Fransson, V., Hagentoft, C-E., (2014). *Influence of heat transfer processes in porous media with air cavity - a CFD analysis*. Submitted to the conference "6th International Conference on Energy Research and Development", March 14-16, 2016, State of Kuwait.
- [15] Shankar, V., Bengtson, A., Fransson, V. Hagentoft, C-E., (2014). *Numerical analysis of the influence of natural convection in attics - a CFD analysis*. Submitted to the conference "6th International Conference on Energy Research and Development", March 14-16, 2016, State of Kuwait.
- [16] Shankar, V., Bengtson, A., Fransson, V. Hagentoft, C-E., (2014). *CFD analysis of heat transfer in ventilated attics*. Submitted to the conference "IAQ 2016 Defining Indoor Air Quality: Policy, Standards and Best Practices", Sept 12 14, 2016, Alexandria, VA.

- [17] Serkitjīs, M. (1995) *Natural convection heat transfer in a horizontal thermal insulation layer underlying an air layer*. Göteborg: Chalmers University of Technology. (PhD Thesis, Department of Building Physics)
- [18] Crowe, C.T., Schwarzkopf, J.D., Sommerfeld, M., Tsuji, Y. (2011). *Multiphase Flows with Droplets and Particles, Second Edition*. CRC Press.
- [19] Versteeg, H.K., Malalasekera, W. (2007) *An Introduction to Computational Fluid Dynamics: the finite volume method*. Pearson Prentice Hall YEAR: 2007
- [20] Andersson, B. et al. (2012) *Computational Fluid Dynamics for Engineers*. Cambridge: Cambridge University Press.
- [21] Davidson, L. (2014) *Fluid mechanics, turbulent flow and turbulence modeling*. Göteborg: Chalmers University of Technology (Lecture Notes, Department of Applied Mechanics)  
<http://www.tfd.chalmers.se/~lada/>
- [22] Çengel, Y.A. (1997) *Introduction to Thermodynamics and Heat Transfer*. New York: McGraw-Hill.
- [23] Wahlgren, P. (2001) *Convection in Loose-fill Attic Insulation*. Göteborg: Chalmers University of Technology. (PhD Thesis, Department of Building Physics)
- [24] ANSYS, Inc. (2011) *ANSYS FLUENT Theory Guide*. Canonsburg: ANSYS, Inc.
- [25] ANSYS, Inc. (2011) *ANSYS FLUENT User's Guide*. Canonsburg: ANSYS, Inc.
- [26] Hagentoft, C-E. (2001). *Introduction to Building Physics*. Studentlitteratur, Sweden.
- [27] Nield, D. A., Bejan, A. (2013) *Convection in Porous Media*. Fourth Edition. New York: Springer
- [28] Ojanen, T., Viitanen, H., Peuhkuri, R. (2007) *Modelling of Mould Growth in Building Envelopes* VTT - Technical Research Center of Finland
- [29] Hamlin, P. (2012). *Modeling of Generation and Distribution of Steam in an Autoclave - A CFD Analysis*. Göteborg: Chalmers University of Technology. (Master's Thesis, Department of Chemical and Biological Engineering)
- [30] Paroc Group. (April, 2014) *Vindsbjälklag Kallvind, b) Med lösullsisolering*.  
<http://www.paroc.se/losningar-och-produkter/losningar/tak/vindsbjalklag-kallvind>
- [31] ROCKWOOL AB. (April, 2014) *CAD-RITNINGAR*.  
<http://www.rockwool.se/v%C3%A4gledning/cad-ritningar>
- [32] Quarrix Building Products. (April, 2014) *The Key to Proper Attic Ventilation*.  
<http://www.quarrix.com/how-quarrix-works/creating-a-balanced-system/>
- [33] MilTyr Avancerade Byggprodukter. (April, 2014) *Ventilationsspringor för taknock och takrygg*.  
<http://www.miltyr.se/index.php?page=takventilation>
- [34] Delmas, A., Arquis, E. (1995). *Early Initiation of Natural Convection in an Opened Porous Layer Due to the Presence of Solid Conductive Inclusions*. Journal of Heat and Mass Transfer, 117, 733-739.

# Appendices

# **Paper 1: Transient Heat Transfer and Moisture Load in Cold Attic Constructions - A CFD Analysis**

# Transient Heat Transfer and Moisture Load in Cold Attic Constructions - A CFD Analysis

V. Shankar<sup>1</sup>, R. Hellsvik<sup>2</sup> & C-E Hagentoft<sup>2</sup>

<sup>1</sup>*ÅF Industry AB, Sweden*

<sup>2</sup>*Division of Building Technology, Chalmers University of Technology, Sweden*

## Abstract

Mold growth in cold attic constructions has become an increasing problem in Sweden and other countries with cold climates due to the demands on energy efficient building envelopes. Highly insulated building envelopes with cold ventilated attics lead to colder climates in the attic space, which increases the risk for mold growth. In this paper, the transient heat transfer process including natural and forced convection is investigated for a 24-hour cycle in a virtual 3D model of a ventilated attic construction by the use of CFD technology. The momentum and energy equations along with the realizable k-epsilon turbulence model are solved with commercial CFD software. Transient simulations are performed for daily temperature variations for various ventilation rates and a hygrothermal analysis is conducted to estimate the risk for mold growth at the inner roof boundary. A virtual model of a ventilated attic with an underlying layer of porous medium is used for the simulations and the CFD approach is based on a validated model from previous research. The results are the temperature field and the risk for mold growth for different ventilation rates presented as a function of time during the cycle.

*Keywords: cold attics, computational fluid dynamics (CFD), heat transfer, moisture load, building physics, fluid mechanics*

## 1 Introduction

In the southern and west part of Sweden, building envelopes that are built or retrofitted with thick insulation layers, are susceptible to mold growth a problem that has increased remarkably over the last decade [1]. The correlation between the local climate and ventilation rates, with the buildup of moisture is of great

interest and recent research [2] shows that greatly reduced, or completely eliminated risk for mold growth can be achieved by controlling the ventilation rate. By investigating the heat transfer process and the flow pattern numerically, knowledge and understanding about their correlation can be obtained in a more efficient way than by performing field measurements. For this investigation the commercial CFD software ANSYS Fluent has been used.

The ventilation in cold attics is usually driven by wind, which forces air into the attic through a gap at one of the eaves (see Figure 1). The ventilated air can then exit the attic through another gap at the opposite side or through an outlet at the top of the roof. The chosen configuration of the ventilation for the attic model is presented in Figure 1, which shows the cross section of the geometry. The attic model is 1800 mm deep in the direction normal to the cross section in Figure 1. The thickest part of the insulation is 400mm and the slope of the roof is 20 degrees. Within the insulation lies wooden joists with spacing of 600 mm, a width of 45 mm and a height of 135 mm, shown in Figure 2. The presence of joists has a significant impact on the heat transfer as well as the flow pattern in the insulation layer [3].

Extensive literature study has shown that the previous research performed so far has only dealt with certain aspects [3, 4, 5, 6, 7, 8, 9, 10, 11, 12]. This CFD attic model was initially developed by the authors in a previous research [10, 11, 12] where it was validated by comparison with experimental work performed by [13].

Data files with hourly measured temperature data from weather stations in Sweden were analyzed and a 24-hour-interval in the middle of April was used to set the external *Dirichlet* boundary conditions for the external air of the attic. Simulations were performed with transient temperatures,  $T_{amb}$  and  $T_{eq}$ , for the ventilated air and the roof boundary respectively, where  $T_{amb}$  denotes ambient temperature and  $T_{eq}$  denotes equivalent temperature which includes effects of solar radiation, long wave radiation, convection and transfer of latent heat. The bottom of the attic floor insulation was set to a constant temperature,  $T_{hot}$ , of 294 K. Three transient simulations were performed for three, constant, inlet velocities corresponding to two, four and eight complete air displacements per hour. The ventilation rates for attics are usually in the range of 0-10 complete air displacements per hour.

The computational mesh was built with hexahedronal elements in the commercial software ANSYS ICEM and a mesh independence study was performed for mesh sizes from 148 000 to 1125 000 computational cells showing that a mesh size of approximately 500 000 cells was sufficient. The Realizable  $k-\epsilon$  model was used to model turbulence in the air cavity while the insulation was modeled as a laminar zone.

## 2 Mathematical Formulation (CFD)

The main equations that have been solved for this problem are the governing equations for conservation of mass, momentum and energy along with the equations for the Realizable  $k-\epsilon$  model with standard wall functions [14]. The P1 model [15] has been used to predict the radiative heat transfer in the domain which solves the transport equation for radiation.

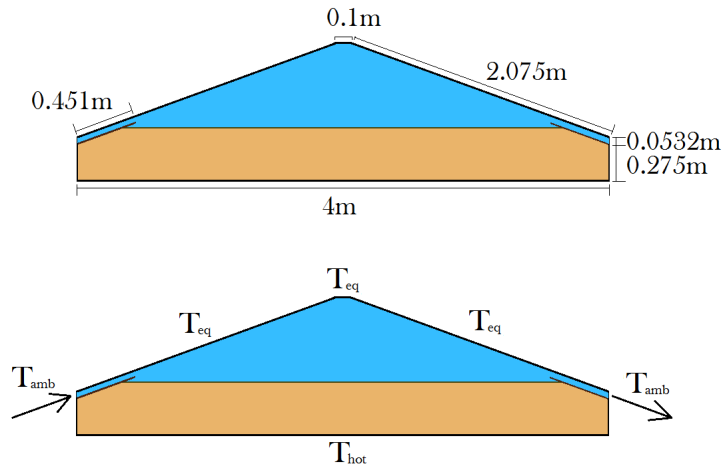


Figure 1: Cross section of the attic model. The upper picture gives the dimensions of the model and the lower picture shows placement of inlet and outlet as well as the temperature boundary conditions. The triangular shaped region represents the air cavity and the lower one the insulation layer.

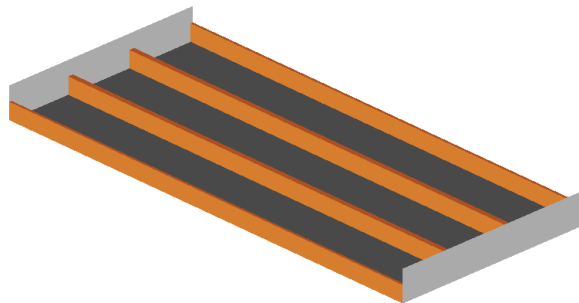


Figure 2: Placement of the wooden joists

## 2.1 Porous Media

The insulated volume is defined as a porous zone in which the porosity  $\phi$  is defined as the fraction of the total volume that is occupied by voids [16]. The volume that is occupied by solid material in a porous medium with porosity,  $\phi$ , is thus  $1 - \phi$ . The porous zone is modeled with the addition of an extra momentum source term,

Equation 1, to the original transport equations consisting of the viscous and inertial losses.

$$S_i = \left( \frac{\mu}{K} u_i + C_2 \frac{1}{2} \rho |u| u_i \right) \quad (1)$$

where  $K$  [m<sup>2</sup>] is the permeability of the insulation material and  $C_2$  [m<sup>2</sup>/kg] is the inertial resistance factor which is usually small compared to the viscous losses for laminar flow, i.e. when the velocities are low. In such cases, the model reduces to Darcys law.  $\mu$  [m<sup>2</sup>/s] is the dynamic viscosity of the fluid,  $u_i$  [m/s] is the local velocity and  $\rho$  [kg/m<sup>3</sup>] is the density of the fluid.

### 3 Relevant Parameters

This section briefly presents the important dimensionless parameters used in this study.

#### 3.1 Nusselt number

The Nusselt number is the ratio between the heat flux with and without convection. It is defined as:

$$Nu = \frac{q_{conduction} + q_{convection}}{q_{conduction}} \quad (2)$$

This parameter is used in this study to describe the impact of convection on the total heat transfer process within the porous medium.

#### 3.2 Humidity and Mold Growth Potential

The relative humidity defined in Equation 3 is used in this study to calculate a potential for the risk of mold growth according to [17]. The mold growth potential,  $m$ , is a number between 0 and 1, corresponding to no growth and initiation of mold growth respectively.

$$RH = \frac{v_a}{v_s} \quad (3)$$

Here,  $v_a$  [g<sub>water</sub>/kg<sub>air</sub>] is the humidity by volume in the attic space including contributions from ventilated air and leakages from the living area through the attic floor. The increase in the humidity level due to leakage from the living area for different ventilation rates is given in Table 1.

$v_s$  [g<sub>water</sub>/kg<sub>air</sub>] is the humidity by volume at saturation approximated as:

$$v_s = \frac{a \cdot \left(b + \frac{T}{100}\right)^n}{461.4 \cdot (T + 273.15)} \quad (4)$$

Table 1: Additional moisture for different ventilation rates

Ventilation rate, $n$	$v_a - v_e$
2	0.3107
4	0.1638
8	0.0842

where  $T$  [ $^{\circ}\text{C}$ ] is the local temperature and  $a$ ,  $b$  and  $n$  are parameters that are constant within certain temperature intervals. The mold growth potential is defined as:

$$m = \frac{RH}{RH_{crit}} \quad (5)$$

where the critical level of the relative humidity is estimated with a polynomial function derived from extensive measurements [17].

## 4 Boundary Conditions

The thermal boundary conditions at the roof, inlet and outlet are prescribed temperature (Dirichlet) and are given by transient tables with measured temperature levels for a 24 h cycle in the middle of April, see Figure 3. The chosen 24-hour cycle was picked out from a large amount of measurements (hourly updated for 30 years) since this interval contained reasonable values to represent the whole month. The data for humidity by volume that came with this specific interval showed to be less representative for the rest of the month since the values are increasing throughout the cycle. It was therefore decided to perform the hygrothermal analysis with a mean value for April (see Figure 6) as input to achieve more general results. The inlet and outlet air is given ambient air temperature and an equivalent temperature is set at the outer roof surface. The floor of the insulation is defined with a constant temperature of 294 K. The boundary conditions of the walls at the short sides of the insulation are given Neumann conditions with a prescribed heat flux set to zero, since this was shown to enhance convergence with very small changes in the results.

## 5 Numerical Setup

The numerical grid was built as a structured mesh in ANSYS ICEM consisting of 500 000 computational cells, which was validated in a mesh independence study as explained in Section 1.

The results presented in this article are achieved with three main simulations for different inlet velocities. To capture the impact of real outdoor conditions they were all conducted as transient simulations with a fixed time step of 1 s and a total time of 86400 s (24 h). A pressure-based solver was used in ANSYS Fluent along

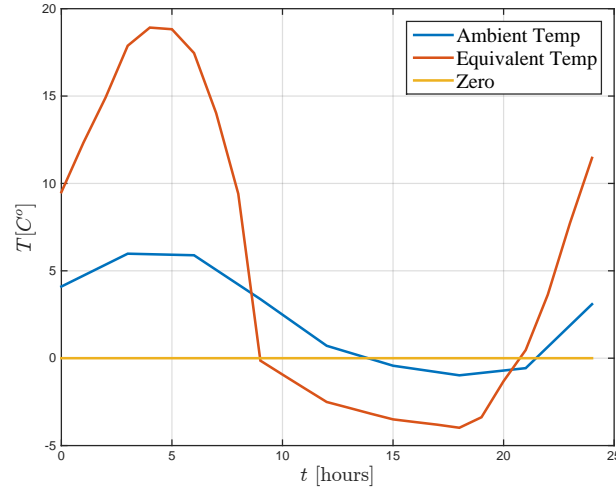


Figure 3: Time dependent ambient and equivalent temperatures taken from measured data plotted together with a line showing the freezing point at atmospheric pressure.

with the implementation of the Boussinesq approximation to capture the buoyancy effects that give rise to natural convection. The numerical scheme SIMPLE was used for pressure-velocity coupling since it was proven to enhance convergence.

To model turbulence in the air space the realizable  $k-\varepsilon$  model with the standard wall function was used, while the flow in the porous zone was assumed to be laminar due to low velocities. Radiation was modeled using the P1 model [15]. The permeability,  $K$ , of the porous medium was set to  $5 \cdot 10^{-8} m^2$ , the porosity,  $\phi$ , to 0.332 and the thermal conductivity,  $k$  [W/(m·K)], of the insulation to 0.044, assumed independent of temperature. These are values that were used when the model was validated by comparison to experimental results [13].

The simulations were initialized with constant boundary conditions for 7200 time steps and the boundary conditions for the roof and ventilation openings were then subsequently read from transient tables. Three main simulations were ran for inlet velocities of 0.0226, 0.0452 and 0.0904 m/s corresponding to 2, 4 and 8 complete air displacements per hour respectively.

Ten monitor points were created along the inner roof boundary to measure the resulting temperature at the inner roof. Each location marked in Figure 4 represents a pair of monitor points with different coordinates in direction parallel to the joists, from which the mean value was taken for analysis. The temperatures at these points were used to estimate the relative humidity and the mold growth potential along the inner roof in the post processing procedure.

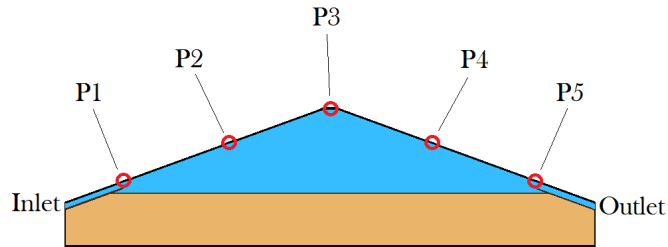


Figure 4: Cross section of the attic model showing the location of the 5 monitor points along the inner roof boundary. Each red mark represents two points in the direction normal to the cross section, one above the center of a joist and one in the middle between two joists.

## 6 Results

The results from the transient simulations are presented in this section.

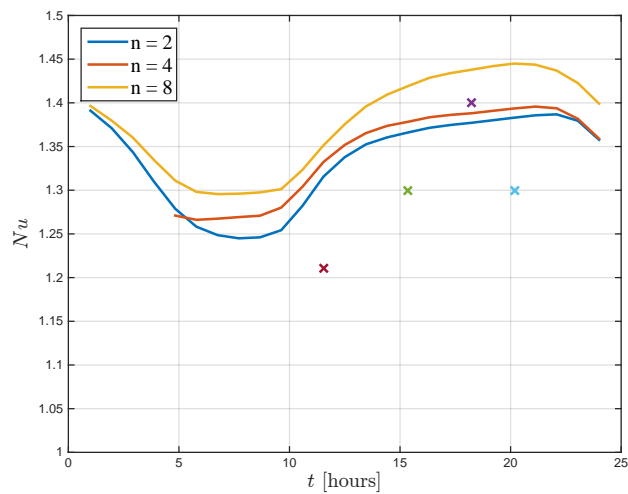


Figure 5: Nusselt number versus time in the insulation layer calculated each hour for all ventilation rates.  $n=2$ ,  $n=4$  and  $n=8$  denotes 2, 4 and 8 complete air displacements per hour respectively. The four crosses show values obtained from experiments with pure natural convection [13].

The Nusselt number in Figure 5 was computed externally in MATLAB by importing data files with node values of temperature for the insulation volume, and cal-

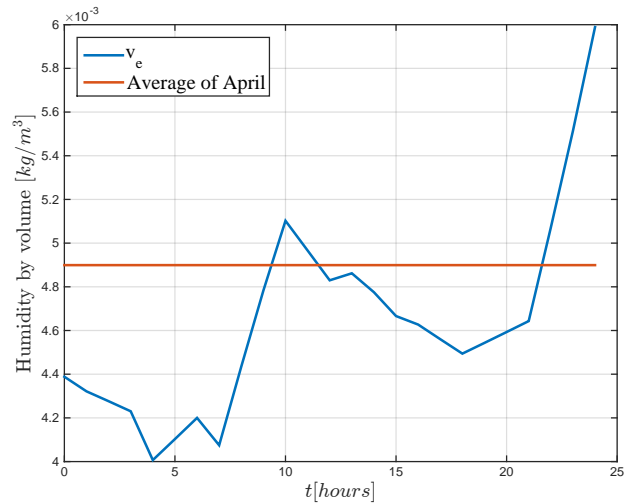


Figure 6: The humidity level in the outdoor air,  $v_e$ , versus time for the chosen day plotted along with the average humidity level for April

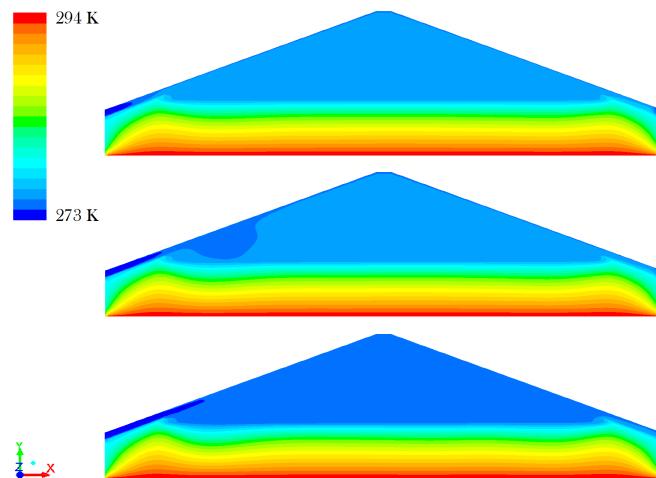


Figure 7: Temperature contours for the middle of the night when the temperature difference is largest, taken in the  $xy$ -plane in the middle of the attic. The plots are for, in order from above, 2, 4 and 8 complete air displacements per hour.

culating the average fraction of the heat flux with and without convection at the heating surface, i.e. the lower surface of the attic floor insulation. One reference simulation was performed with the momentum and turbulence equations disabled in order to achieve values for the heat flux without the presence of convection, rep-

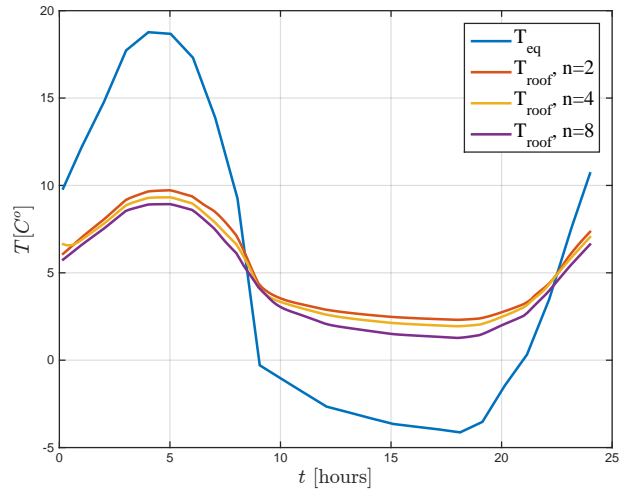


Figure 8: The boundary condition for the roof boundary,  $T_{eq}$ , versus time, plotted along with the mean temperature of the inner roof for the three ventilation rates.

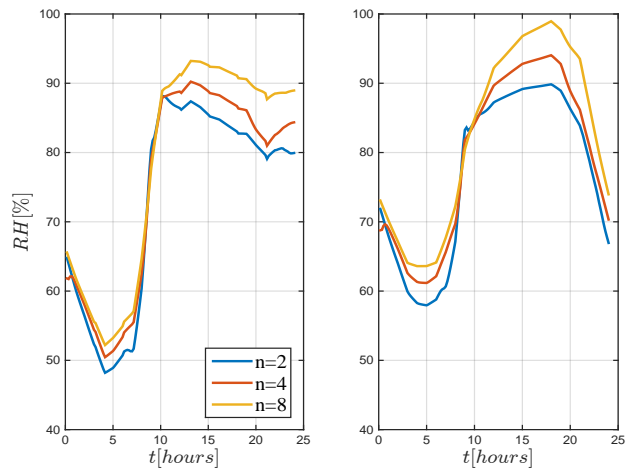


Figure 9: Relative humidity versus time measured at location P1 (see Figure 4). The left plot shows the values calculated from the time dependent  $v_e$  and the right plot shows values from the averaged one, and the same goes for Figure 10, 11, 12 and 13.

resenting the denominator of Equation 2, and the three cases for different air flows yielded input for the numerator.

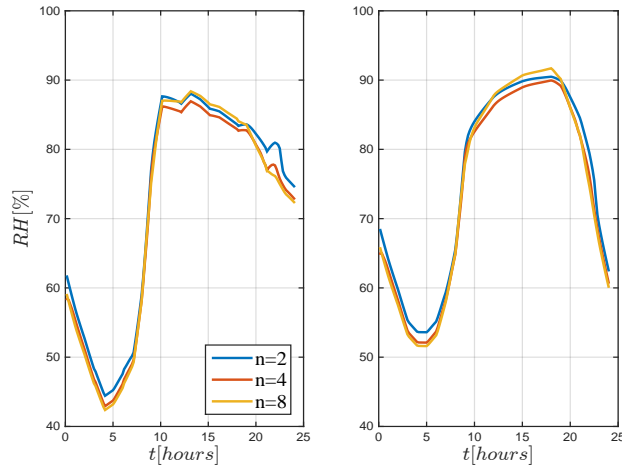


Figure 10: Relative humidity versus time measured at location P2.

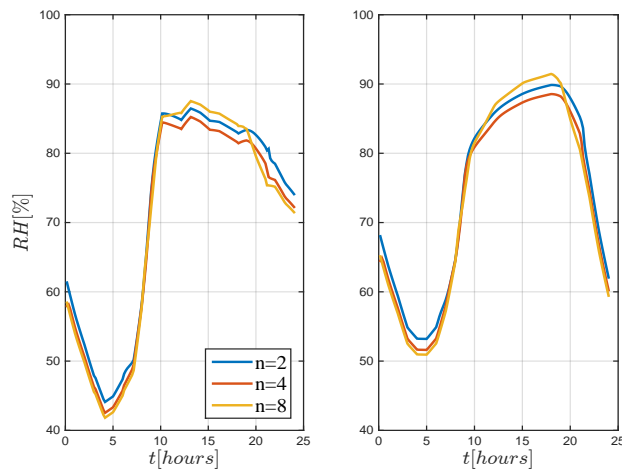


Figure 11: Relative humidity versus time measured at location P3.

The temperature contours in Figure 7 give understanding about the temperature distribution in the domain for different ventilation rates at the coldest point of the cycle. In Figure 7 it is seen that as the ventilation rate increases, a cloud of cold air spreads along the roof starting at the inlet. The same is proven by Figure 8 where the average temperature at the inner surface of the roof is plotted for different ventilation rates.

The levels of relative humidity and the mold growth potential are presented in two separate plots in Figure 9-18. The left plots in each figure show values

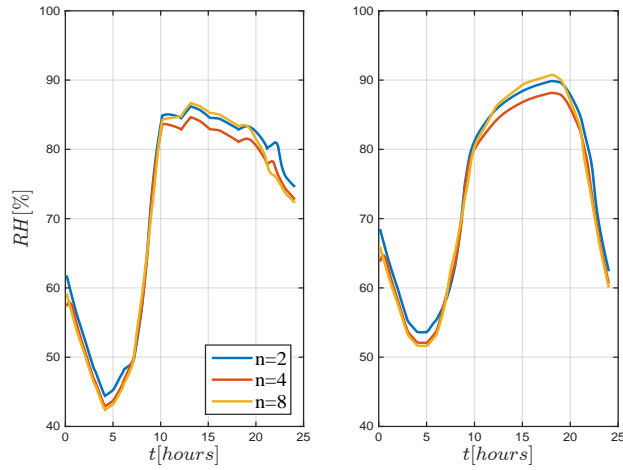


Figure 12: Relative humidity versus time measured at location P4.

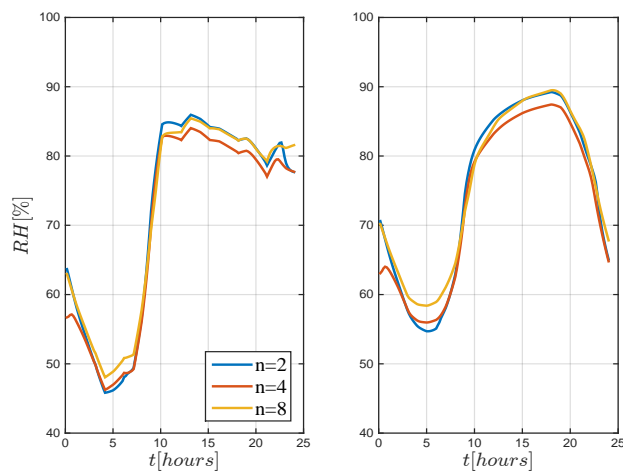


Figure 13: Relative humidity versus time measured at location P5.

calculated from the actual measured moisture content of the ventilated air, and the plots on the right side corresponds to the average humidity by volume for the whole month of April, as shown in Figure 6.

## 7 Discussion

As seen in Figure 5 and 8, the temperature difference between the inner roof surface and the bottom of the attic floor insulation has a large impact on the convec-

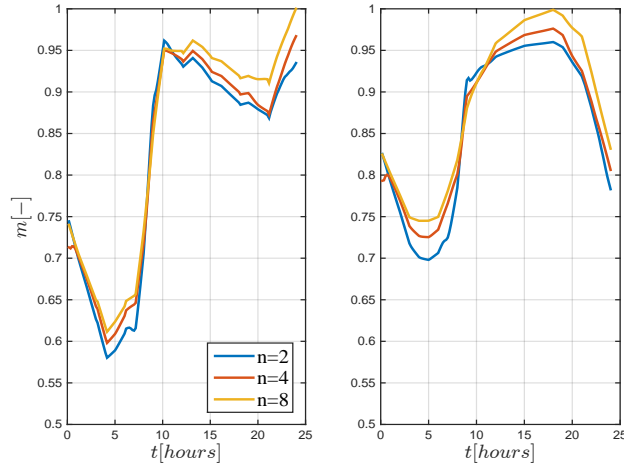


Figure 14: Mold growth potential,  $m$ , versus time measured at location P1 (see Figure 4). The left plot shows the values calculated from the time dependent  $v_e$  and the right plot shows values from the averaged one, and the same goes for Figure 15, 16, 17 and 18.

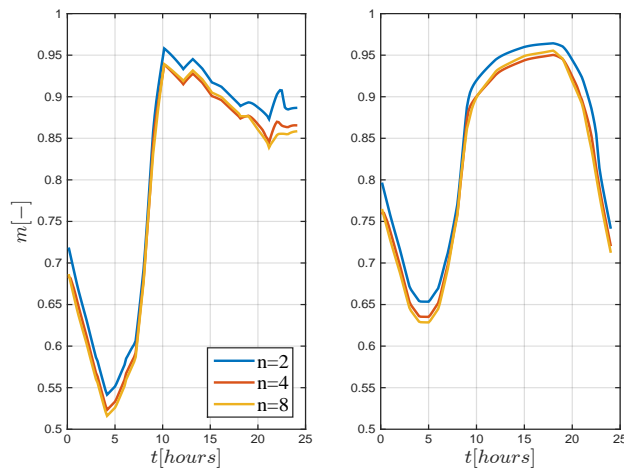


Figure 15: Mold growth potential,  $m$ , versus time measured at location P2.

tive heat transfer in the insulation. For the chosen cycle the conditions are such that convective heat transfer is always present in the porous medium but with varying magnitude. It is also concluded that the ventilation rate magnifies the convective transport of heat in the insulation layer, leading to a greater heat flux from the living area as the ventilation rate is increased. By studying the Nusselt number, we

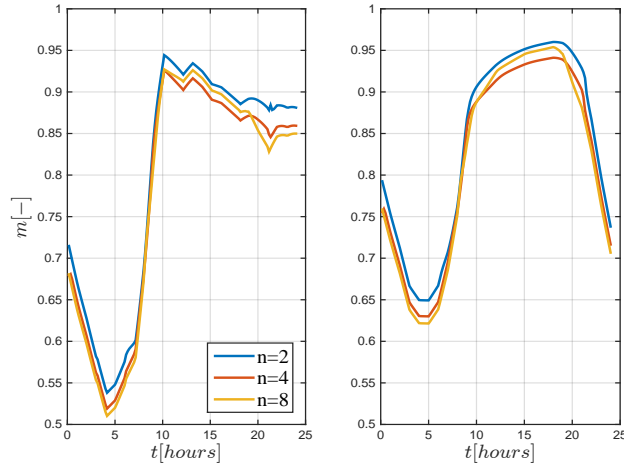


Figure 16: Mold growth potential,  $m$ , versus time measured at location P3.

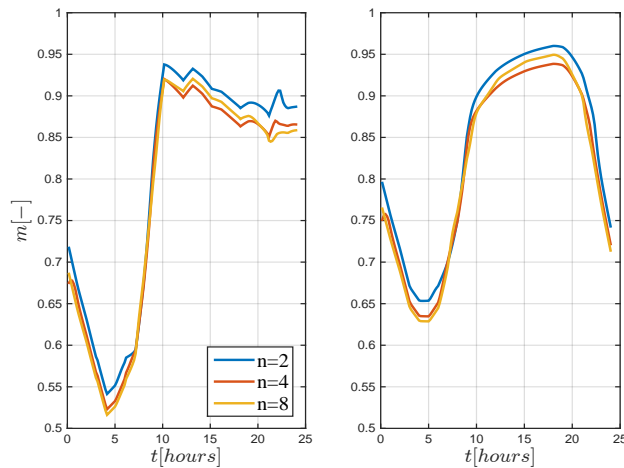


Figure 17: Mold growth potential,  $m$ , versus time measured at location P4.

are provided with information about the possible draw backs in terms of energy efficiency when optimizing the ventilation rate for minimal mold growth, since higher ventilation rates has a negative impact in the energy efficiency of the building. The four points in Figure 5 are values of the Nusslet number from experiments in a previous study [13]. The temperature difference over the insulation was used to determine the modified Rayleigh number according to the results in the experiments and the Nusslet numbers for those Rayleigh numbers were then added to the plot as a validation. These experiments were performed for pure natural con-

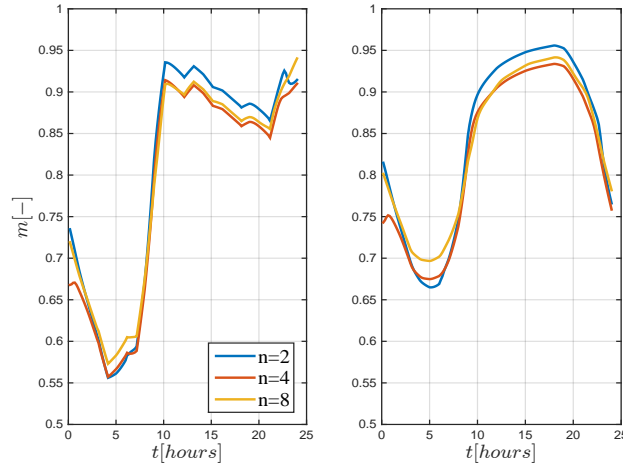


Figure 18: Mold growth potential,  $m$ , versus time measured at location P5.

vection which is a reason why the values for the Nusselt number from that study are slightly lower. Since there are currently no experimental results from measurements with the climatic conditions investigated in this study, the validity of the CFD model relies on the validation performed in [10]

Figure 5 shows that the Nusselt number exceeds 1 for all air displacements proving that convective heat transfer takes place in the porous medium. From Figure 5 it can be seen, glancing at Figure 3, that as the temperature difference between the roof and the floor increases, the magnitude of heat transfer due to convection also increases in the insulation. It is also noticed that the convective heat transfer gets slightly more dominant for higher ventilation rates.

As mentioned in Section 6, the low temperature of the ventilated air is spreading from the inlet through the attic, while in the air cavity the air is heated by the rising heat from below. For low ventilation rates ( $n = 2$ ) the air is heated up to a slightly higher temperature before it reaches the air cavity, and as the ventilation rate increases the cold air is able to travel a longer distance before it is heated up. In the contour in the middle of Figure 7 (4 complete air displacements per hour), the cold region has just reached the air cavity and a cloud of cold air is visible near the lower part of the left roof boundary, and for 8 complete air displacements per hour the cloud has spread throughout the air cavity. This tells us that the part of the roof closest to the inlet suffers the greatest risk for mold related problems.

The same can be seen by analyzing the levels of relative humidity and mold growth potential in Figure 9 to Figure 18. It is concluded that the part of the roof close to the inlet (P1 in Figure 4) is exposed to the greatest risk for mold related problems among the analyzed locations.

Finally, it should be understood that these results are taken for one specific day of the year and they are applied to one out of many attic designs, which makes

these results very specific for the studied model.

## 8 Conclusion

The simulations yield reasonable results for the studied case. The simulations show that the heat flux in the insulation is affected by the ventilation rate leading to a slightly less energy efficient building for higher ventilation rates due to the convective heat transfer. Going from 2 to 8 complete air displacements per hour increases the heat flux through the floor of the attic by approximately 5%. The obtained values of the Nusselt number are in line with previous experiments.

The relative humidity and the mold growth potential is highest at locations close to the inlet when the ambient temperature is low. At location P1 by the inlet, the highest mold growth potential ( $\sim 1$ ) is found for the highest ventilation rates, while the lowest ventilation rate yields the highest risk for mold growth for the rest of the locations.

## 9 Future Work

When this model was validated by comparison with experiments it was concluded that the total heat transfer in the porous medium is over predicted by Fluent, due to the inability of the code to account for resistance to radiative heat transfer in the porous zone. An investigation regarding alternative solutions for this problem is needed to achieve better accuracy of the results.

It is also of great interest to apply the tools developed in this research project on other attic designs and different inlet-outlet-configurations to optimize the ventilation strategies for minimal mold growth.

## Acknowledgment

This research project has been conducted with financial resources provided by ÅForsk, ÅF Industry AB, Sweden and the Division of Building Technology, Chalmers University of Technology.

## References

- [1] Jönsson, B. et al., Så mår våra hus, 2009.
- [2] Hagentoft, C.E. & Kalagasidis, A.S., Mold growth control in cold attics through adaptive ventilation. validation by field measurements. *Proceedings of the XI International Conference on the Performance of the Exterior Envelopes of Whole Buildings*, 2010.
- [3] Delmas, A. & Wilkes, K., Numerical Analysis of Heat Transfer by Conduction and Natural Convection in Loose-Fill Fiber Glass Insulation Effects of Convection on Thermal Insulation. *ORNL/CON-338*.
- [4] Wahlgren, P., *Convection in Loose-fill Attic Insulation*. PhD Thesis, Chalmers

University of Technology, Göteborg, 2001.

- [5] Wahlgren, P., Measurements and simulations of natural and forced convection in loose-fill attic insulation. *Journal of Thermal Envelope and Building Science*, **26**, pp. 93–109, 2002.
- [6] Shankar, V. & Hagentoft, C.E., Influence of natural convection on the thermal properties of insulating porous medium with air cavity. *Indoor air 99, Edinburgh*.
- [7] Shankar, V. & Hagentoft, C.E., Numerical investigation of natural convection in Horizontal porous media heated from below Comparisons with experiments. *ASME International, Pittsburgh*.
- [8] Shankar, V., Davidson, L. & Olsson, E., Numerical Investigation of Turbulent Plumes in both Ambient and Stratified Surroundings. *Journal of INDOOR AIR, Denmark*.
- [9] Shankar, V., Davidson, L. & Olsson, E., Ventilation by Displacement: Calculation of Flow in Vertical Plumes. *ROOM VENT, Aalborg, Denmark*.
- [10] V. Shankar, B., A & Fransson, V., Influence of Heat Transfer Processes in Porous Media with Air Cavity - A CFD Analysis. *Submitted to the conference "6th International Conference on Energy Research and Development", March 14-16, 2016, State of Kuwait*.
- [11] V. Shankar, B., A & Fransson, V., Numerical Analysis of the Influence of Natural Convection in Attics - A CFD Analysis. *Submitted to the conference "6th International Conference on Energy Research and Development", March 14-16, 2016, State of Kuwait*.
- [12] V. Shankar, B., A & Fransson, V., CFD Analysis of Heat Transfer in Ventilated Attics. *Submitted to the conference "IAQ 2016 Defining Indoor Air Quality: Policy, Standards and Best Practices", Sept 12-14, 2016, Alexandria, VA*.
- [13] Serkitjäs, M., *Natural convection heat transfer in a horizontal thermal insulation layer underlying an air layer*. PhD Thesis, Chalmers University of Technology, Göteborg, 1995.
- [14] Andersson, B. & et al, *Computational Fluid Dynamics for Engineers*. Cambridge University Press: Cambridge, 2012.
- [15] ANSYS, Inc, *ANSYS FLUENT Theory Guide*. ANSYS, Inc, Canonsburg, latest edition.
- [16] Nield, D. & Bejan, A., *Convection in Porous Media*. Springer: New York, 2013.
- [17] T. Ojanen, R.P., H. Viitanen, Modelling of Mold Growth. VTT - Technical Research Centre of Finland, 2007.

# **Paper 2: Transient Modeling of Heat Transfer and Evaporation in Cold Attics - A CFD Analysis**

# Transient Modeling of Heat Transfer and Evaporation in Cold Attics - A CFD Analysis

V. Shankar<sup>1</sup>, R. Hellsvik<sup>2</sup> & C-E Hagentoft<sup>2</sup>

<sup>1</sup>*ÅF Industry AB, Sweden*

<sup>2</sup>*Division of Building Technology, Chalmers University of Technology, Sweden*

## Abstract

Due to climatic changes and the present design of highly insulated buildings, microbial growth has become an increasing problem in cold attics in the southern and west part of Sweden. This paper is a continuation of a previous research where the transport of air and moisture was investigated in a cold attic construction. Numerical modeling of condensation and evaporation at the roof boundary is performed with the Eulerian Wall Film Model in the commercial CFD software ANSYS Fluent. The impact of different ventilation rates on the water film thickness is being investigated. The model contain a ventilated triangular shaped airspace with an underlying layer of insulation where conductive and convective heat transfer takes place. Contours of water film thickness, static temperature and mass fraction of water in the air cavity is presented as functions of the Reynolds number in the results.

*Keywords: cold attics, computational fluid dynamics (CFD), heat transfer, moisture load, eulerian wall film model, building physics, fluid mechanics*

## 1 Introduction

In a previous research [1], transient heat transfer in a cold attic model was numerically investigated for a 24 hour cycle with typical Swedish climatic conditions of the month of April. The numerical results were used to determine the relative humidity and the mold growth potential by the use of mathematical models derived from extensive experiments. This article is a continuation of the research work performed by the authors in the previous paper [1], which in turn is based on previous research [2, 3, 4, 5, 6, 7, 8, 9, 10, 11, 12]. Numerical modeling of the condensation

and evaporation of water at the inner roof boundary is performed to estimate how the moisture load is affected by different ventilation rates of the attic. The same geometry, mesh and numerical setup is conducted, and the addition of the Eulerian Wall Film Model [13] is used to investigate condensation at one of the roof boundaries for the part of the 24 hour cycle which, in the previous research, showed to be the most critical. The commercial CFD software ANSYS Fluent is used for the simulations.

The heat transfer process in attics usually include both natural and forced convection due to the gaps on the side of the attic where air can flow in over the wind deflectors. There are different ventilation configurations for attic constructions and in this model the roof boundary is sealed and an outlet is placed at the opposite side as seen in fig. 1.

Simulations were performed with a constant temperature,  $T_{hot}$ , of 294 K at the bottom of the attic. The thermal boundary conditions for the roof was set to  $T_{eq}$ , corresponding to the equivalent surface temperature of the roof including the cooling effects of sky radiation. The temperature of the ventilated air,  $T_{amb}$ , was set to ambient air temperature. The values of these temperatures represent clear sky conditions for the coldest part of the chosen 24 hour cycle (see fig. 2) and they are presented in table 1.

Transient simulations with constant boundary conditions has been performed for 4 different ventilation rates in a range from 2 to 8 complete air displacements per hour and the results, in terms of water film thickness as functions of Reynolds number after a certain amount of time steps are compared.

The CFD model was initially validated for steady state simulations by comparison with experimental results [14] when it was developed by the authors of a previous articles [1, 9, 10, 11].

## 2 The Eulerian Wall Film Model

The Eulerian Wall Film model (EWFm) is a model used to estimate the creation and flow of liquid films that build up on wall surfaces, in this case due to condensation. This model is to be used when the thickness of the film is small compared to the radius of the surface curvature, and when the film is thin enough so that the flow within the film can be assumed to be parallel to the surface.

The fundamentals of the liquid film is based on a two dimensional film and the foundation of the EWFm is formed by the governing equations for conservation of mass and momentum. For a two dimensional Wall Film in a three dimensional domain the conservation of mass reads:

$$\frac{\partial H}{\partial t} + \nabla_s \cdot [H \vec{V}_l] = \frac{\dot{m}_s}{\rho_l} \quad (1)$$

where  $H$  is the thickness of the film,  $\nabla_s$  is the surface gradient operator,  $\vec{V}_l$  is the mean film velocity which is very low in the studied case,  $\rho_l$  is the density of the liquid and  $\dot{m}_s$  is the mass source per unit wall area due to incoming droplets, film

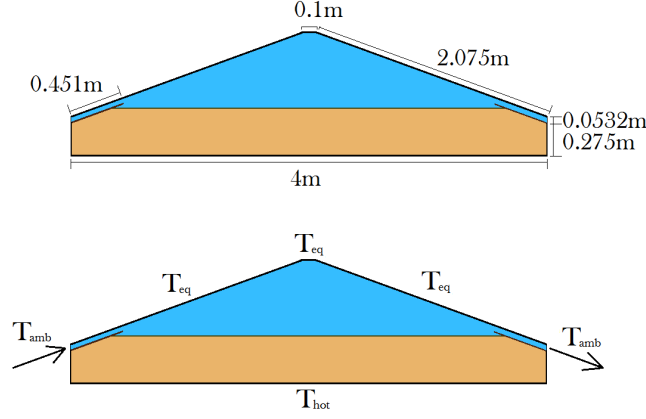


Figure 1: Cross section of the attic model. The upper picture gives the dimensions of the model and the lower picture shows placement of inlet and outlet as well as the temperature boundary conditions. The triangular shaped region represents the air cavity and the lower one the insulation layer.

separation, film stripping and phase change.

The conservation of film momentum reads:

$$\frac{\partial H \vec{V}_l}{\partial t} + \nabla_s \cdot (H \vec{V}_l \vec{V}_l) = -\frac{H \nabla_s p_L}{\rho_l} + (\vec{g} \cdot \vec{\tau}) H + \frac{3}{2\rho_l} \vec{\tau}_{fs} - \frac{3v_l}{H} \vec{V}_l + \frac{\dot{q}}{\rho_l} \quad (2)$$

where

$$p_L = p_{gas} + p_h + p_\sigma = p_{gas} + (-\rho H (\vec{n} \cdot \vec{g})) + (-\sigma \nabla_s \cdot (\nabla_s H)) \quad (3)$$

The terms on the left hand side in equation 2 are transient and convection effects, respectively. The first term on the right hand side represents the gas-flow pressure, the gravity component normal to the surface, and the surface tension. The second term includes the gravity effects parallel to the wall. The third and fourth terms represents the viscous shear force at the interface with the gas and within the film respectively. The last term is the droplet collection or separation.

In case of thermal modeling the conservation of film energy is also needed:

$$\frac{\partial (HT_f)}{\partial t} + \nabla_s \cdot (\vec{V}_f HT_f) = \frac{1}{\rho C_p} \left[ 2k_f \left[ \frac{T_s + T_w}{H} - \frac{2T_f}{H} \right] + \dot{q}_{imp} + \dot{m}_{vap} L(T_s) \right] \quad (4)$$

where  $T_s$  is the surface temperature of the film,  $T_f$  is the average film temperature,  $T_w$  is the solid wall temperature.  $\dot{q}_{imp}$  is the source term due to impingement of droplets into the film,  $\dot{m}_{vap}$  is the rate of mass condensation or vaporization and  $L$

Table 1: Main boundary conditions for temperatures and moisture content,  $v_e$ , of the ventilated air.

Roof	$T_{eq} = 269.17 \text{ K}$
Floor	$T_{hot} = 294 \text{ K}$
Inlet	$T_{amb} = 272.17 \text{ K}$ , $v_e = 3.9 \text{ g}_{\text{water}}/\text{kg}_{\text{air}}$
Outlet	$T_{amb} = 272.17 \text{ K}$

is the latent heat associated with phase change of the liquid. [13]

Note that this is not a multiphase model and should therefore be used when the volume fraction of the dispersed phase is negligible in the bulk flow. In ANSYS Fluent, species are defined so that the water content of the ventilated air is included in the model. This model was chosen since it is the most efficient way to model moisture transport for a cold attic where condensation of water takes place only at the walls.

### 3 Numerical Setup

The numerical setup used for the simulations is identical to that in the previous article [1] except for the boundary conditions, which are time independent in this study. The boundary conditions include prescribed temperatures at the roof, inlet, outlet and at the bottom of the insulation according to table 1 and the inlet also has a prescribed mass fraction of water. All values are taken from the coldest time of the transient tables that were used in [1]. The side walls perpendicular to the joints have a prescribed heat flux of  $q = 0$ , and symmetry boundary conditions are set for the walls parallel to the joints. The outlet was defined as a pressure outlet boundary with atmospheric pressure.

The time step for the main equations was set to 1 s and for the Eulerian Wall Film a time step of 0.2 s was defined. While running the simulations the film thickness was monitored and the simulations were ran until the film thickness had reached a steady value. 5 different inlet velocities were investigated corresponding to 2, 4, 5, 6 and 8 complete air displacements per hour.

### 4 Results

The results from the simulations are presented in this section.

The simulations were performed with constant boundary conditions and were ran for approximately 20000 time steps which corresponds to approximately 5.5 hrs. Each case was initiated with a film thickness of 0.5 mm and the results show the drying effect of the ventilated air for different Reynolds numbers, at a surface that is already wet. Contours of static temperature and mass fraction of water are plot-

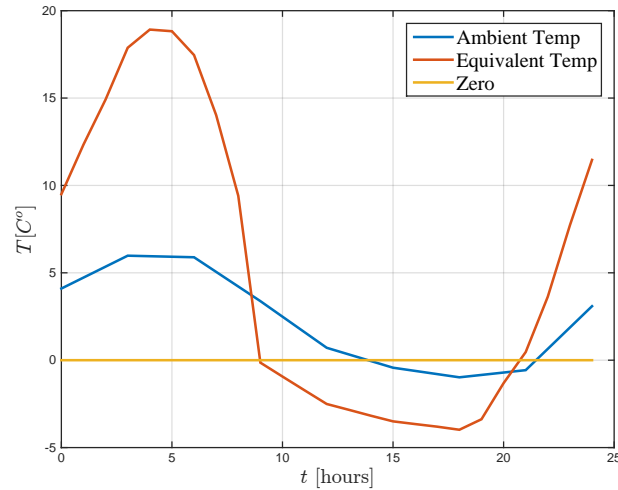


Figure 2: Time dependent ambient and equivalent temperatures taken from measured data

ted in a cross section plane in the middle of the domain, and water film thickness is plotted in a top view of the roof boundary closest to the inlet.

Fig. 3 shows the temperature contours for the  $xy$ -plane in the middle of the domain. All four contours in the figure show the temperature field at a time that correspond to the middle of the night where the temperature difference between the roof and the floor is largest. The same structure is seen in fig. 4 where the mass fraction of water in the domain is plotted. For all ventilation rates, it is seen that the highest mass fraction of water is found close to the left side of the roof boundary where the wall film was activated due to evaporation of water.

In fig. 5 the wall film thickness is plotted in a top view of the left side of the roof. A zone of water concentration is found in a region positioned where the wind shields end and as the inlet velocity increases this zone is pushed further away from the inlet. Another zone where the film is thicker is found at the top of the roof. The maximum film thickness was also monitored and plotted (see fig. 6) as functions of the Reynolds number to overview the variations.

## 5 Discussion

The contours of mass fraction of water in fig. 4 shows a clear difference in humidity close to the left roof boundary for different ventilation rates. The reason why the left roof boundary has a significantly higher level of humidity is mostly because of the Eulerian Wall Film model being activated at that surface. Due to limitations in computational resources it was not possible solve the wall film model for all boundaries.

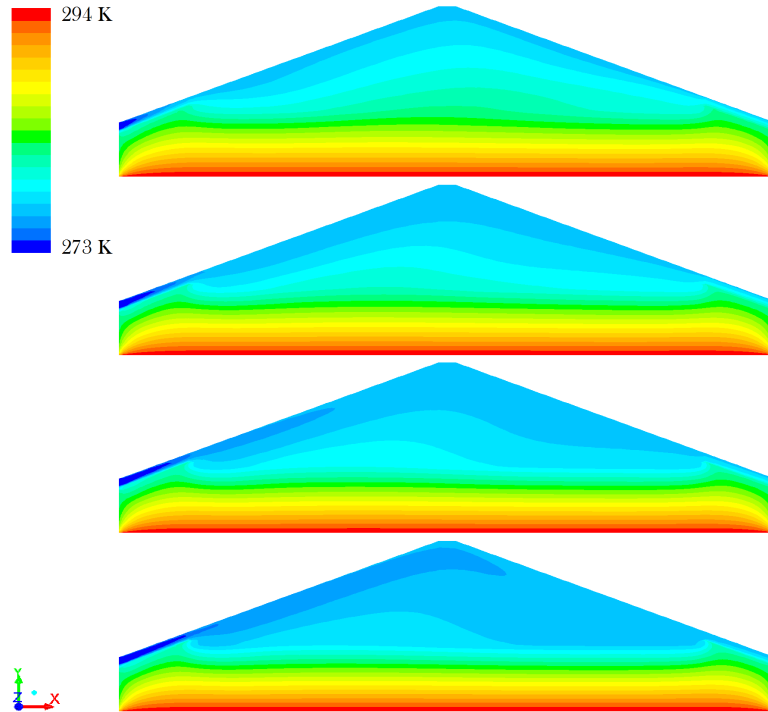


Figure 3: Temperature contours in a cross section in the middle of the attic for different ventilation rates. The pictures represent, from above, 2, 4, 6 and 8 complete air displacements per hour respectively.

The temperature plots were presented in this article to see if the temperature field would be affected by the presence of an Eulerian Wall Film, by comparing the temperature contours with the ones that were presented in [1] where a region of cold air was seen close to the left roof boundary. The same behavior was found in this study but with a slightly different distribution. The differences most likely have to do with the fact that the simulations in the previous article [1] were run with continuously varying boundary conditions while the simulations in this study have had constant conditions for all boundaries.

By looking at the trend line of the maximum thickness in fig. 6 it is seen that a minimum thickness is found for  $Re \approx 260$  after which the maximum thickness starts to increase. It should, however, be noted that the maximum thickness for  $n=2$ ,  $n=4$  and  $n=6$  appears in the region in the middle part of the roof, and that the maximum thickness for  $n=8$  appears at the left edge of the roof. If the maximum thickness of the middle region would have been plotted instead, the trend line would be continuously decreasing for increasing Reynolds numbers.

These results represent the physics of this specific attic design and the same results cannot be assumed to be valid for other designs or other climatic conditions.

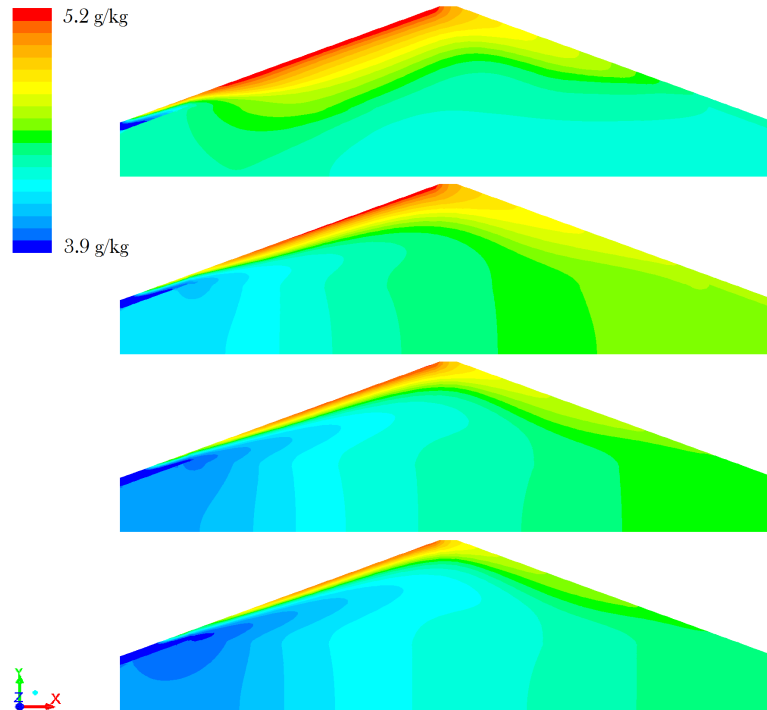


Figure 4: Contours of mass fraction of water [ $g_{water}/kg_{air}$ ] in a cross section in the middle of the attic for different ventilation rates. The pictures represent, from above, 2, 4, 6 and 8 complete air displacements per hour respectively.

Furthermore it should be understood that the surface of the roof boundary is treated by Fluent as a wall without any absorption of water.

## 6 Conclusion

The simulations give physical results for the studied case. The lowest ventilation rate yield the highest value of the film thickness but a large part of the roof that is completely dry. As the ventilation rate increases the maximum thickness is reduced but a larger part of the roof is covered with water. The maximum thickness that was found in this research was approximately 1.23 mm and while some parts of the roof will be "dry" even though the case was initialized with a film of constant thickness over the whole surface.

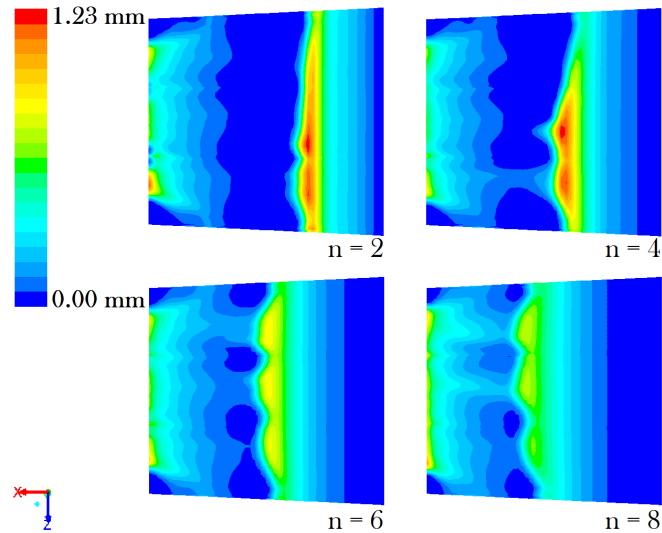


Figure 5: Contours of Eulerian Wall Film thickness plotted at the roof of the attic closest to the inlet for different ventilation rates. The right edge of each figure is the edge where the inlet and the roof meet, and the left edge of each figure is the top of the roof. The pictures represent, from above, 2, 4, 6 and 8 complete air displacements per hour respectively.

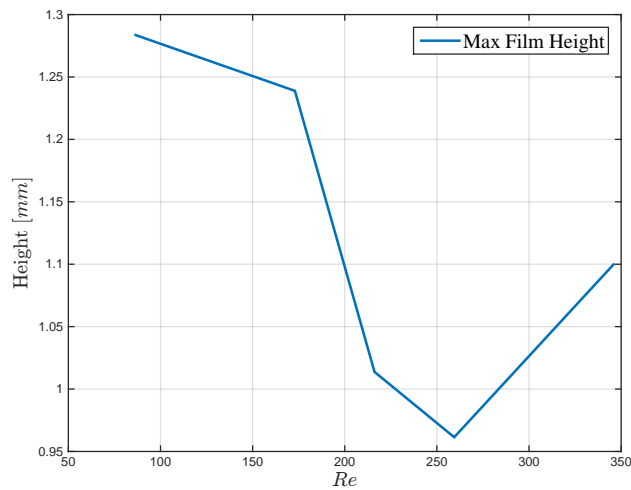


Figure 6: Maximum values for film thickness plotted for different Reynolds numbers corresponding to 2, 4, 5, 6 and 8 complete air displacements per hour.

## 7 Future Work

To be able to make a comparison between this way of modeling moisture load and the way described in [1] it is needed to model absorption of the roof boundary and to run simulations with the same transient boundary conditions. It is also needed to activate the Eulerian Wall Film model for the whole roof - something that was not possible during this study due to time limitations.

Furthermore, To provide valuable information about prediction of mold growth it is needed to perform this kind of simulations for various attic designs and for boundary conditions that represent other climatic conditions. It would then be possible to optimize the ventilation rate for minimal mold growth, for different buildings.

## Acknowledgment

This research project has been conducted with financial resources provided by ÅForsk, ÅF Industry AB, Sweden and the Division of Building Technology, Chalmers University of Technology.

## References

- [1] V. Shankar, C.H., R. Hellsvik, Transient Heat Transfer and Moisture Load in Cold Attic Constructions - A CFD Analysis. *Submitted to the conference "6th International Conference on Energy Research and Development", March 14-16, 2016, State of Kuwait, 2015.*
- [2] Delmas, A. & Wilkes, K., Numerical Analysis of Heat Transfer by Conduction and Natural Convection in Loose-Fill Fiber Glass Insulation Effects of Convection on Thermal Insulation. *ORNL/CON-338.*
- [3] Wahlgren, P., *Convection in Loose-fill Attic Insulation.* PhD Thesis, Chalmers University of Technology, Göteborg, 2001.
- [4] Wahlgren, P., Measurements and simulations of natural and forced convection in loose-fill attic insulation. *Journal of Thermal Envelope and Building Science*, **26**, pp. 93–109, 2002.
- [5] Shankar, V. & Hagentoft, C.E., Influence of natural convection on the thermal properties of insulating porous medium with air cavity. *Indoor air 99, Edinburgh.*
- [6] Shankar, V. & Hagentoft, C.E., Numerical investigation of natural convection in Horizontal porous media heated from below Comparisons with experiments. *ASME International, Pittsburgh.*
- [7] Shankar, V., Davidson, L. & Olsson, E., Numerical Investigation of Turbulent Plumes in both Ambient and Stratified Surroundings. *Journal of INDOOR AIR, Denmark.*
- [8] Shankar, V., Davidson, L. & Olsson, E., Ventilation by Displacement: Calculation of Flow in Vertical Plumes. *ROOM VENT, Aalborg, Denmark.*

- [9] V. Shankar, B., A & Fransson, V., Influence of Heat Transfer Processes in Porous Media with Air Cavity - A CFD Analysis. *Submitted to the conference "6th International Conference on Energy Research and Development", March 14-16, 2016, State of Kuwait.*
- [10] V. Shankar, B., A & Fransson, V., Numerical Analysis of the Influence of Natural Convection in Attics - A CFD Analysis. *Submitted to the conference "6th International Conference on Energy Research and Development", March 14-16, 2016, State of Kuwait.*
- [11] V. Shankar, B., A & Fransson, V., CFD Analysis of Heat Transfer in Ventilated Attics. *Submitted to the conference "IAQ 2016 Defining Indoor Air Quality: Policy, Standards and Best Practices", Sept 12-14, 2016, Alexandria, VA.*
- [12] Lejon, M., *Wall Condensation Modelling in Convective Flow*. Master's Thesis, KTH, Industrial Engineering and Management, Stockholm, Sweden, 2013.
- [13] ANSYS, Inc, *ANSYS FLUENT Theory Guide*. ANSYS, Inc, Canonsburg, latest edition.
- [14] Serkitjäs, M., *Natural convection heat transfer in a horizontal thermal insulation layer underlying an air layer*. PhD Thesis, Chalmers University of Technology, Göteborg, 1995.